

Article

Thermodynamic Optimization of Advanced Organic Rankine Cycle Configurations for Geothermal Energy Applications

Nenad Mustapić¹, Vladislav Brkić^{2,*}, Željko Duić² and Toni Kralj¹¹ Karlovac University of Applied Sciences, Trg Josipa Jurja Strossmayera 9, 47000 Karlovac, Croatia² Faculty of Mining, Geology and Petroleum Engineering, University of Zagreb, Pierottijeva 6, 10000 Zagreb, Croatia

* Correspondence: vladislav.brkic@rgn.unizg.hr

Abstract: The Organic Rankine Cycle (ORC) is commonly accepted as a viable technology to convert from low to medium temperature geothermal energy into electrical energy. In practice, the reference technology for converting geothermal energy to electricity is the subcritical simple ORC system. Over time, geothermal ORC plants with more complex configurations (architectures) have been developed. In the open literature, a large number of advanced architectures or configurations have been introduced. An analysis of the scientific literature indicates that there is some confusion regarding the terminology of certain advanced ORC system architectures. A new categorization of advanced configurations has been proposed, with a special emphasis on the application of geothermal energy. The basic division of advanced plant configurations is into dual-pressure and dual-stage ORC systems. In this study, the real potential of advanced ORC architectures or configurations to improve performance as compared with the simple ORC configuration was explored. The research was conducted for a wide range of geothermal heat source temperatures (from 120 °C to 180 °C) and working fluids. Net power output improvements as compared with the basic subcritical simple ORC (SORC) configuration were examined. The ability to produce net power with different ORC configurations depends on the magnitude of the geothermal fluid temperature and the type of working fluid. At a lower value of geothermal fluid temperature (120 °C), the most net power of 18.71 (kW/(kg/s)) was realized by the dual-pressure ORC (DP ORC configuration) with working fluid R1234yf, while the double stage serial-parallel ORC configuration with a low-temperature preheater in a high-temperature stage ORC (DS parHTS LTPH ORC) generated 18.51 (kW/(kg/s)) with the working fluid combination R1234yf/R1234yf. At 140 °C, three ORC configurations achieved similar net power values, namely the simple ORC configuration (SORC), the DP ORC configuration, and the DS parHTS LTPH ORC configuration, which generated 31.03 (kW/(kg/s)) with R1234yf, 31.07 (kW/(kg/s)) with R1234ze(E), and 30.96 (kW/(kg/s)) with R1234ze(E)/R1234yf, respectively. At higher values of geothermal fluid temperatures (160 °C and 180 °C) both the SORC and DP ORC configurations produced the highest net power values, namely 48.58 (kW/(kg/s)) with R1234ze(E), 67.23 (kW/(kg/s)) with isobutene for the SORC configuration, and 50.0 (kW/(kg/s)) with isobutane and 69.67 (kW/(kg/s)) with n-butane for the the DP ORC configuration.

Keywords: Organic Rankine Cycle; dual-pressure ORC; double stage serial-parallel ORC configuration; geothermal energy



Citation: Mustapić, N.; Brkić, V.; Duić, Ž.; Kralj, T. Thermodynamic Optimization of Advanced Organic Rankine Cycle Configurations for Geothermal Energy Applications.

Energies **2022**, *15*, 6990.

<https://doi.org/10.3390/en15196990>

Academic Editor: Frede Blaabjerg

Received: 16 August 2022

Accepted: 18 September 2022

Published: 23 September 2022

Publisher's Note: MDPI stays neutral with regard to jurisdictional claims in published maps and institutional affiliations.



Copyright: © 2022 by the authors. Licensee MDPI, Basel, Switzerland. This article is an open access article distributed under the terms and conditions of the Creative Commons Attribution (CC BY) license (<https://creativecommons.org/licenses/by/4.0/>).

1. Introduction

In the future, mass production of electricity from renewable sources is planned to achieve the set targets of reducing CO₂ emissions and other greenhouse gases into the Earth's atmosphere. One of the largest sources of renewable energy is geothermal energy. Geothermal energy is renewable energy obtained by using heat from the interior of the Earth. It has been estimated that, at earth depths up to 3000 m, there are 43,000,000 EJ of geothermal energy [1] stored. The temperatures of geothermal sources range from

50 °C to 350 °C. Medium and low enthalpy geothermal resources are usually found in continental regions and are largely widespread. Astolfi et al. [2] determined that low and medium enthalpy geothermal fields had temperature limits from 120 °C to 180 °C. Low and medium enthalpy geothermal resources represent attractive sources for electrical power production. When low and medium water-dominated geothermal resources are available, binary cycle (indirect) power plants can be used. It is estimated that 70% of the total geothermal sources belong to water-dominated low and medium enthalpy resources with temperatures below 150 °C [3]. In binary power plants, two thermodynamic cycles are used, namely the Organic Rankine Cycle (ORC) and Kalina Cycle (KC) [4]. Binary power plants use low boiling working fluids that are more suitable to use under these geothermal conditions [5,6]. A comparative thermodynamic analysis between the Organic Rankine Cycle (ORC) and Kalina Cycle (KC) systems have shown that the ORC system achieves higher work production and better cost-effectiveness at low and medium temperature heat sources (from 90 °C to 150 °C) [7].

LeCompte et al. [8] reviewed advanced ORC architectures (or configurations) for waste heat recovery (WHR), and multiple evaporation pressures (MP) were among the proposed advanced ORC configurations. The authors asserted that multi-pressure Organic Rankine Cycle plants had not been analyzed extensively in the open literature.

The basic idea of a two-stage evaporation strategy is to improve system performance by decreasing the irreversibility involved in the heat transfer process between the heat source fluid and working fluid in an ORC plant. Therefore, heat is transferred into the ORC plant, and due to the irreversibility reduction in the cycle, more net power is generated. There is a good temperature match between the heat source fluid high-temperature side and the working fluid high-pressure evaporation conditions in the high-temperature ORC stage. The same conclusion is valid for the heat source fluid low temperature side and the low pressure evaporation conditions in the low temperature ORC stage.

The two-stage evaporation strategy can be realized in two different ways. The first way is to divide the flow of the working fluid in the ORC plant into two parts. The first part of the working fluid flow, which is compressed by the pump to the appropriate high pressure, exchanges heat with the heat source fluid at its inlet temperatures. After that, the heat source fluid exchanges heat with the other part of the working fluid flow, which is under a correspondingly lower pressure (and temperature). This is referred to as the high-pressure (HP) and low-pressure (LP) parts of the ORC plant. In the literature, these types of plants are most often called dual-pressure (DP) or two pressure level ORC configurations. Another way is that the heat source fluid exchanges heat with two separate ORC plants (or stages). The heat source fluid exchanges heat with the first stage, which has the high temperatures necessary to achieve the appropriate temperature match. Therefore, this first ORC stage is called the high-temperature stage (HTS). Then, the heat is exchanged with another ORC stage that has correspondingly low temperatures. This stage of the ORC plant is called the low-temperature stage (LTS). Such ORC plants are commonly referred to as double stage (DS) ORC configurations, since they consist of a high-temperature stage (HTS) and a low-temperature stage (LTS) in which the working fluids may or may not be the same.

In recent years, the thermodynamic performance of dual-pressure (DP) ORC configurations has been extensively investigated. Stijepovic et al. [9] emphasized that it was possible to achieve significant improvements in a plant's performance (as compared with the standard SORC) by introducing multiple pressures. They also concluded that the addition of a third pressure level did not provide significant improvements in ORC plant performance. There were several variants within the DP ORC configurations with respect to the arrangement of pumps and turbines in the plant. It was determined by the analyses that the best DP ORC plant performance was achieved with a serial arrangement of low-pressure and high-pressure pumps [10] and a serial or induction arrangement of high-pressure and low-pressure turbines [11]. Guzovic et al. [12] determined that, in the case of the geothermal field Velika Ciglena (175 °C), the DP ORC configuration achieved slightly lower thermal efficiency, but considerably higher both exergy efficiency and net power output as compared

with a simple ORC (SORC) plant. Manante et al. [13] conducted a comprehensive comparison of the thermodynamic characteristics of SORC and DP ORC configurations under subcritical conditions for geothermal heat sources in the temperature range from 100 °C to 200 °C. At lower geothermal fluid temperatures (100–125 °C), the net power output from the DP ORC was considerably higher, but at higher geothermal fluid temperatures (150–200 °C) this advantage of the DP ORC configuration was significantly reduced.

Double stage (DS) ORC configurations can be divided into three basic groups, which differ in the distribution of the heat flow exchange between the heat source fluid and the working fluids in the individual stages. In the first group of DS ORC plants, serial heat exchange takes place between individual stages of the ORC plant and the heat source fluid (serial DS ORC group). First, the HTS exchanges heat with the heat source fluid, followed by the LTS. HTS and LTS can be realized with or without an internal heat exchanger (IHE). In the serial DS ORC group, we have the following configurations: serial DS ORC with an IHE in an HTS (DS HTSIHE ORC) [14], serial DS ORC with an IHE in an LTS (DS LTSIHE ORC) [15], serial DS ORC with an IHE in an HTS and an LTS (DS 2×IHE ORC) and serial DS ORC with two SORCs (DS 2×SORC) [16].

In the second group of DS ORC plants, serial-parallel heat exchange takes place between individual stages of the ORC plant and the heat source fluid (serial-parallel DS ORC group). The serial-parallel DS ORC configuration can be performed in two ways. In the first, variant heat is first exchanged serially between the heat source fluid and the HTS and LTS; this is followed by parallel additional preheating of the working fluids in both stages. Therefore, high-temperature (HT) and low-temperature (LT) preheaters (PH) exist in both ORC stages. The flow of the heat source fluid is divided (after preheating the working fluid in the HTPH in the LTS) in the appropriate ratios, and then each parallel flow heats the working fluid in the low-temperature preheaters (LTPHs) in each stage of the ORC plant. This variant of the plant can be called the DS serial-parallel ORC configuration with LTPHs in both ORC stages (DS par2×LTPH ORC). Kanoglu [17] conducted an exergy analysis of a geothermal power plant that operates commercially in Nevada (USA) and has a DS par2×LTPH ORC configuration. Heberle et al. [18] performed a thermodynamic analysis of the commercial geothermal power plant Kirchstockach (Germany), in which another variant serial-parallel DS ORC configuration was made. In this configuration, the serial heat exchange was completed in the LTS evaporator. After that, the heat source fluid flow was divided into two parts. The heating of the working fluid in the LTS preheater and the HTS low-temperature preheater (LTPH) was performed in parallel modus. After that, these two flows merged again and were pumped into the ground through the reinjection well. This variant of the plant configuration can be called the DS serial-parallel ORC configuration with a LTPH in an HTS ORC (DS parHTSLTPH ORC). In this variant of the ORC configuration there was a single-stage preheating of the working fluid in the LTS. The authors of same paper concluded (after the analysis of the scientific literature) that there was some confusion regarding the terminology of certain advanced ORC system configurations. Consequently, a categorization of advanced two-stage evaporation ORC configurations was proposed in this article, which is shown in Table 1. Liu et al. [19] performed an exergy analysis for this ORC configuration, which has been rarely considered in the scientific literature, especially for geothermal heat sources.

Table 1. Categorization of advanced two-stage evaporation ORC configurations (wf, working fluid).

| Advanced two-stage evaporation ORC configurations | DP | Serial Pump Arrangements and Serial or Induction Turbine Arrangement | | | | 1×WF | |
|---|----|--|-------------------|---------------|-------------------|---------------|--------------|
| | | serial | DS HTSIHE ORC | DS LTSIHE ORC | DS 2×IHE ORC | DS 2×SORC ORC | |
| | DS | ser./par. | DS parHTSLTPH ORC | | DS par2×LTPH ORC | | 1×WF or 2×WF |
| | | cascaded | DS casLTSPH ORC | | DS casnoLTSPH ORC | | |

In the third group of DS ORC plants, cascaded heat exchange takes place between individual stages of the ORC plant (cascaded DS ORC group). In the cascaded DS ORC configuration, the condenser of the upper stage high-temperature stage (HTS) acts as the

evaporator and preheater of the lower stage low-temperature stage (LTS). One variant of this configuration is the DS casnoLTSPH ORC, in which the entire heat for preheating and evaporation of the low-temperature stage (LTS) is provided through condensation of the working fluid in the high-temperature stage (HTS). Another variant is the DS casLTSPH ORC, in which the working fluid in the LTS is partially preheated using a heat source fluid after the HTS and the rest of the heat is supplied by the HTS condenser. The cascaded ORC configuration has been proposed for waste heat recovery [20,21] (DS casnoLTSPH ORC) and for power production from geothermal sources [22] (DS casLTS PH ORC).

In this paper, the thermodynamic characteristics of the selected ORC configurations are compared in such a way that the maximum values of the net power output are determined as the goal of the optimization process. The thermodynamic characteristics of the following four configurations are compared: simple ORC (SORC), dual-pressure ORC (DP ORC), double stage (DS) serial-parallel ORC configuration with a low-temperature preheater (LTPH) in a high-temperature stage (HTS) ORC (DS parHTSLTPH ORC), and serial double stage (DS) ORC with an internal heat exchanger (IHE) in a high-temperature stage (HTS) ORC (DS HTSIHE ORC). Heat sources are low and medium enthalpy geothermal fields that have temperatures from 120 °C to 180 °C. All ORC plants have a mode of operation in subcritical conditions, and the working fluids must be environmentally friendly. To the best of our knowledge, in the scientific literature, there is no thorough systematic assessment of the thermodynamic potential of the suggested ORC configurations suitable for the production of electrical energy from geothermal sources. This claim was supported by a previous study of the published literature, in which certain configurations of ORC geothermal plants had been mainly analyzed as stand-alone systems at certain temperatures of geothermal sources, or some of the configurations had been analyzed as industrial waste heat recovery systems. Therefore, a comprehensive analysis has not been conducted on the electrical energy production potential of the selected ORC configuration in different geothermal conditions.

2. Methodology

2.1. System Description

In this paper, the characteristics of four configurations of ORC geothermal plants were studied. The selected configurations of the ORC plants are shown in Figure 1, while their corresponding Ts diagrams (temperature-entropy) are shown in Figure 2. The simplest configuration of the present ORC plants is the simple ORC, shown in Figure 1a (thermodynamic scheme) and Figure 2a (Ts diagram). Thermal energy from the geothermal flow is transferred to the working fluid in the superheater, evaporator, and preheater. Then, the geothermal water is reinjected back into the geothermal well. The produced working fluid vapor goes to the turbine where the energy taken from the working fluid is converted into mechanical work, and in the electric generator the generated mechanical work is converted into electricity. After the turbine, the working fluid is brought to the initial thermodynamic state by cooling with air (or water) in the desuperheater, condenser, and subcooler, and then compressed in the pump to the evaporation pressure.

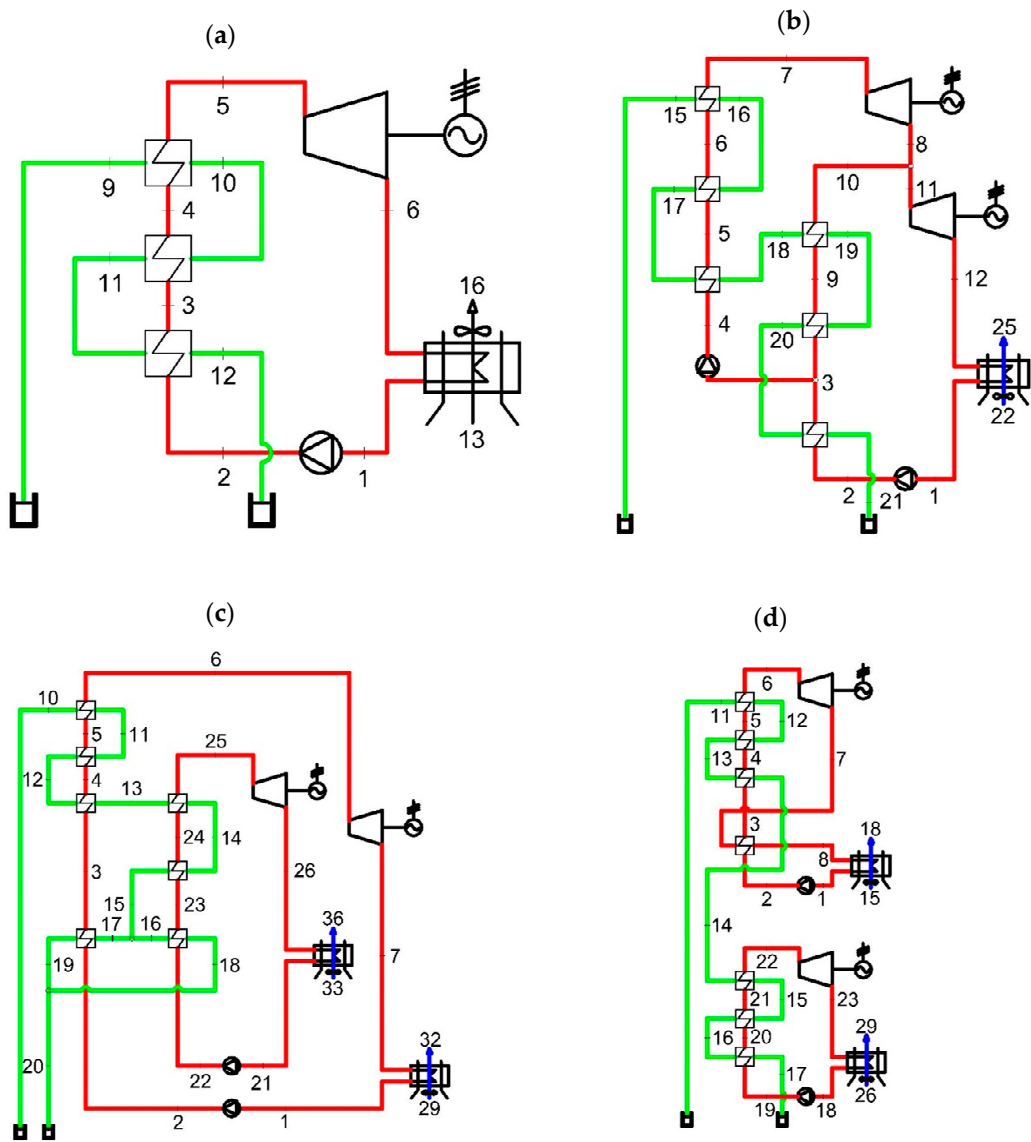


Figure 1. Analyzed ORC configurations: (a) SORC; (b) DPORC; (c) DS parHTSLTPH ORC; (d) DS HTSIHE ORC.

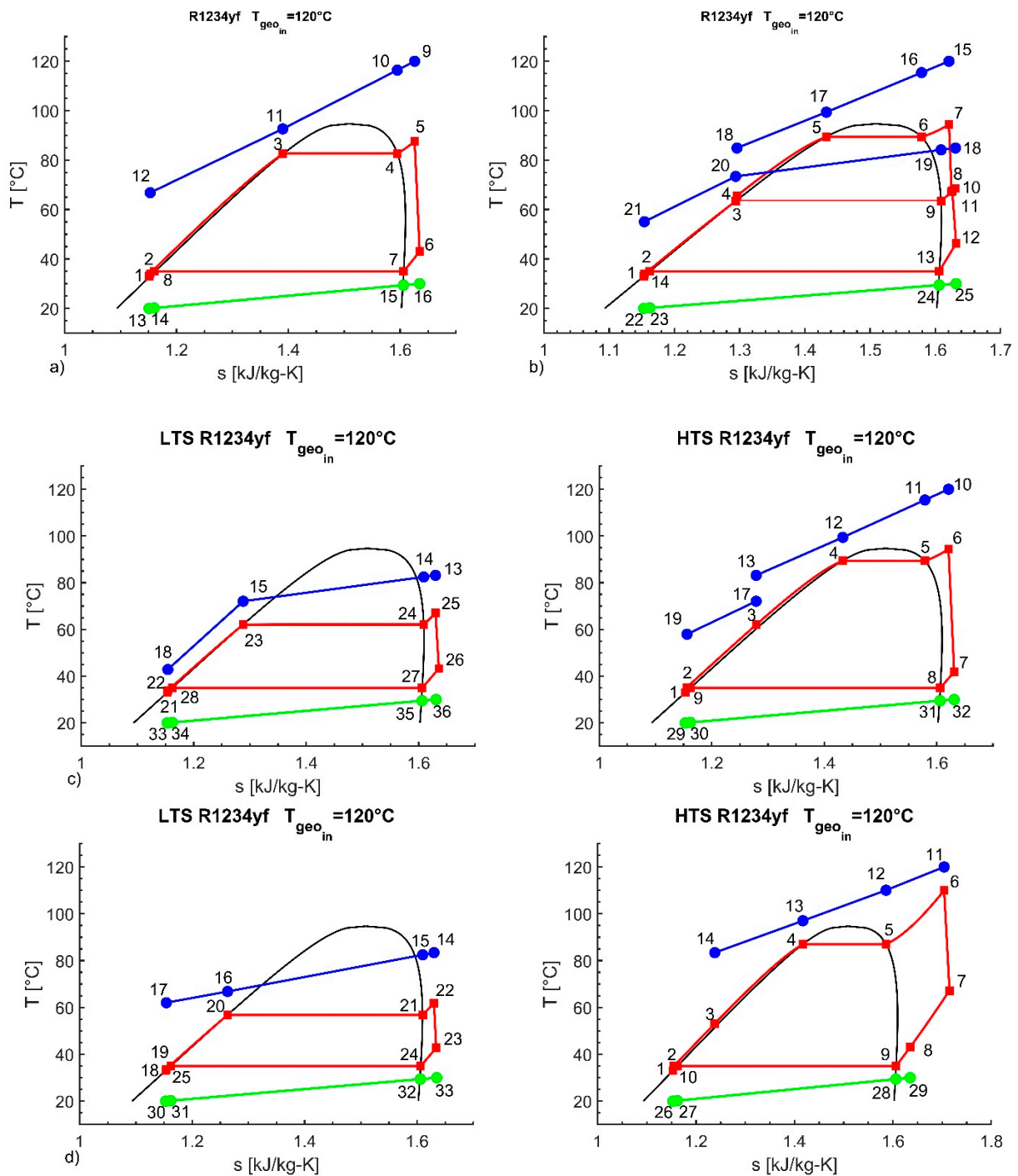


Figure 2. Ts diagrams of analyzed ORC configurations: (a) SORC; (b) DP ORC; (c) DS parHTS LTPH ORC; (d) DS HTSIHE ORC.

The dual-pressure ORC configuration (DP ORC) is shown in Figure 1b, while its corresponding Ts diagram is shown in Figure 2b. As the name suggests, in this configuration, the process of heat exchange between the geothermal fluid and working fluid takes place under two working pressures (i.e., high and low). The total working fluid flow is compressed to low pressure (LP) by means of a low-pressure pump (LPP). After that, the total working fluid flow is heated in a low-pressure preheater (LPPH), after which the working fluid flow is separated into low-pressure flow and high-pressure flow. Thermal energy from the geothermal flow is exchanged, first, with the high-pressure working fluid

flow in the high-pressure superheater (HPSH), evaporator (HPEV), and preheater (HPPH), and then with the low-pressure working fluid flow in the low-pressure superheater (LPSH), evaporator (LPEV), and preheater (LPPH). After that, the geothermal fluid is reinjected into the geothermal well. This ORC configuration has a serial or induction turbine arrangement, which means that the high-pressure fluid flow (after superheating) enters the high-pressure turbine (HPT) where it expands to low pressure. The output flow from the HPT is mixed with the low-pressure working fluid flow, and this joint flow enters the low-pressure turbine (LPT), where it expands to the condenser pressure. After the LPT, the total working fluid flow goes to the air-cooled condenser (or cooling tower) where it condenses and is subcooled. The subcooled working fluid flow in the low-pressure pump (LPP) is compressed to low pressure.

The double stage serial-parallel ORC configuration with a low-temperature preheater in a high-temperature stage (DS parHTS LTPH ORC) is shown in Figure 1c, while its corresponding Ts diagram is shown in Figure 2c. The mentioned configuration consists of two separate ORC plant stages: the high-temperature stage (HTS) and the low-temperature stage (LTS). In each of the ORC stages, there can be the same working fluid, or different working fluids. The geothermal fluid exchanges heat with the working fluid in the high-temperature stage (HTS), first, with the superheater (HTSSH), then with the evaporator (HTSEV), and finally with the high-temperature preheater (HTSHTPH). After that, the geothermal fluid exchanges heat with the working fluid in the low-temperature stage (LTS), first, with the superheater (LTSSH), and then with the evaporator (LTSEV). After leaving the LTSEV, the geothermal fluid flow is divided into two separate flows. First, the geothermal flow goes to the low-temperature stage preheater (LTSPH), while the other geothermal flow goes to the high-temperature stage low-temperature preheater (HTSLTPH). After preheating, both geothermal flows are mixed again, and the geothermal fluid is injected into the geothermal well. The specificity of this ORC configuration is two-level preheating (low-temperature preheating and high-temperature preheating) of the working fluid in an HTS and parallel low-temperature preheating of working fluids in an HTS and an LTS by dividing the geothermal fluid flow into two parts. The HTS and LTS have their own turbines, condensers, and circulation pumps.

The serial double stage ORC configuration with internal heat exchanger (IHE) in a high-temperature stage (DS HTSIHE ORC) is shown in Figure 1d, while its corresponding Ts diagram is shown in Figure 2d. This configuration consists of two separate ORC plant stages: a high-temperature stage (HTS) and a low-temperature stage (LTS). The HTS has an internal heat exchanger (IHE) or recuperator, and the LTS is the SORC cycle. Ss in the previous ORC configuration in each ORC stage can be the same working fluid, or can be the different working fluids in different stages. The geothermal fluid, first, exchanges heat with the working fluid in the HTS (superheater, evaporator, and preheater), and finally with the working fluid in the LTS. After that, the geothermal fluid is injected into the geothermal well. The HTS and LTS have their own turbines, condensers, and circulation pumps.

2.2. Thermodynamic Modeling and Assumptions

The selected configurations of the ORC geothermal systems were simulated using computer programs developed using the Engineering Equation Solver (EES) software, version 9.370 published by F-Chart Software, Madison, WI, USA [23]. Each component of the system was defined as a control volume for which the principles of mass conservation and the first and second laws of thermodynamics were applied.

The ORC plant thermodynamic performance could be evaluated when values of all model variables were defined. The fixed variables, or model parameters, were assumed prior to calculation and kept constant in the thermodynamic optimization procedure. The design variables, or independent variables, were determined by the optimization routine. The model parameters used in all simulations are reported in Table 2.

Table 2. Model parameters used in the simulations for all stimulation.

| | | |
|---|--------|--------------------|
| Pump isotropic efficiency | (%) | 70 |
| Turbine isotropic efficiency | (%) | 85 |
| Pump and turbine mechanical efficiency | (%) | 95 |
| Condenser cooling medium | - | Air |
| Geothermal heat source temperature | (°C) | 120/140/160/180 |
| Evaporator pinch point | (°C) | 10 |
| Condenser pinch point | (°C) | 5 |
| Condensation temperature | (°C) | 35 |
| Mass flow value of the heat source medium | (kg/s) | 1 |
| Pressure of the heat sink medium | (bar) | 1 |
| Temperature of the heat sink medium | (°C) | 20 |
| Pressure of the heat source medium | (bar) | 10 |
| Heat source medium | - | (geothermal) water |
| Subcooling temperature difference | (°C) | 2 |

About ten years ago, the ORC plant with supercritical parameters was built in Italy, and in the USA there were three such plants. Although in recent years ORC plants with supercritical parameters have aroused significant interest in the scientific community, no development projects of such plants have been recorded in commercial practice. Therefore, we chose to study only the thermodynamic characteristics of ORC plants with subcritical working fluid conditions. The evaporation pressures in all ORC configurations could have maximum values which were 10% lower than the critical pressure for the specified working fluid.

In the selected ORC configurations, some technical details were provided to ensure safe operation of the plants. Therefore, the ORC configurations were all equipped with superheaters and subcoolers.

Superheating of working fluid negatively affects the efficiency of an ORC plant with dry fluid, positively affects an ORC plant with wet fluid, and almost does not affect an ORC with isentropic fluid [24]. An experimental observation by [25] indicated that superheating was necessary even for dry working fluid, due to the appearance of the liquid entrainment phenomenon. The superheating of the working fluid was also necessary due to the regulations of the ORC plant. Therefore, the selected ORC configurations all had working fluid superheaters as a standard plant component. The minimum value of the working fluid overheating was 5 °C.

The main circulation pump was installed at the outlet of the condenser. However, the working fluid at the outlet of the condenser was in a saturated liquid state, which meant that its pressure was equal to the vapor pressure. The vapor pressure is the pressure (at the appropriate temperature) at which the liquid begins to boil or evaporate. In such a situation, cavitation occurs in the main circulation pump. Cavitation is the formation and sudden compression of steam bubbles in the pump, because evaporation of the working fluid occurs due to the pressure drop below the vapor pressure. Long-term operation of the pump in cavitation mode can significantly damage the pump. This means that a sufficiently high pressure must be ensured in front of the main circulation pump, or the temperature of the working fluid in front of the pump must be sufficiently reduced. The required pressure can be achieved by creating a static pressure difference by positioning the main circulation pump vertically, sufficiently below the condenser. Such an intervention is difficult to carry out in practice without a significant increase in material costs. Another solution is to install a heat exchanger—subcooler that can achieve thermal subcooling of the working fluid in front of the main circular pump. Subcooling is undesirable in terms of system efficiency,

but it is necessary in order to exclude main circular pump cavitation. It was assumed that subcooling of 2 °C (ΔT_{SC} in Table 1) was sufficient to prevent cavitation in the system.

It is envisaged that condensation (desuperheating, condensation, and subcooling) takes place in air-cooled condensers. In the literature [26] it has been suggested that the air cooling process required a power input in the range of 0.5–1.25 kW to remove 100 kW of the heat. In all simulations, 1 kW input power per 100 kW of the removed heat was considered to be the correct value.

In the mathematical model formulations for all of the ORC configuration systems, the following assumptions are made:

1. The mass flow rate of the working fluid in all considered ORC configurations is 1.0 kg/s;
2. The systems operate in a steady-state condition;
3. Changes in kinetic and potential energies are neglected;
4. The pumps and the turbines operate adiabatically with appropriate isentropic and mechanical efficiencies, as given in Table 2;
5. Pressure losses are neglected through the heat exchangers and in the pipelines;
6. The geothermal field is considered to be a water-dominated reservoir and geothermal brine is assumed to be a saturated liquid state.

2.2.1. Energy System Models and Assumptions

Mass and energy balances for each component of the selected configurations of geothermal systems at steady-state conditions are:

$$\sum \dot{m}_{in} = \sum \dot{m}_{out} \quad (1)$$

$$\dot{Q} + \dot{W} = \sum \dot{m}_{out} h_{out} - \sum \dot{m}_{in} h_{in} \quad (2)$$

where the subscripts in and out represent the inlet and outlet states, respectively; \dot{Q} and \dot{W} are the net heat and work inputs, respectively; \dot{m} is the mass flow; and h is the specific enthalpy. The relationship for each component for the SORC and DP ORC configurations are given in Table 3 and the relations for each component in Appendix A, Table A1. The relations for each component (first law analysis) for the DS parHTSLTPH ORC and DS HTSIHE ORC configurations are given in Appendix A, Table A2.

Table 3. Model parameters used in the simulations for the SORC and DP ORC configurations.

| Name | P_{cr} (bar) | T_{cr} (°C) | Safety Group | ODP | GWP |
|------------------------|----------------|---------------|--------------|---------|-----|
| Cyclopentane | 45.15 | 238.54 | A3 | 0 | 11 |
| N-pentane R601 | 33.6 | 196 | n.a. | 0 | 20 |
| Isopentane (ic5) R601a | 33.78 | 187.2 | A3 | 0 | 20 |
| Neopentane R601b | 31.96 | 160.6 | n.a. | 0 | 20 |
| R1233zd(E) | 35.7 | 165.6 | A1 | 0.00034 | 7 |

Table 3. Cont.

| Name | P _{cr} (bar) | T _{cr} (°C) | Safety Group | ODP | GWP |
|--------------------------|-----------------------|----------------------|--------------|-----|------|
| R245fa | 36.51 | 154.01 | B1 | 0 | 1050 |
| R1234ze(Z) | 35.3 | 153.7 | A2L | 0 | 6 |
| n-butane R600 | 37.9 | 152 | A3 | 0 | 3 |
| isobutane (ic4) R600a | 36.29 | 135 | A3 | 0 | 3.3 |
| R1234ze(E) | 36.4 | 109.4 | A2 | 0 | 6 |
| R134a | 40.59 | 101 | A1 | 0 | 1430 |
| R1234yf | 33.8 | 94.7 | A2Lr | 0 | 4.4 |

2.2.2. Conventional Exergy System Models

Exergy of each stream in the ORC system (\dot{E}) consists of four different parts:

$$\dot{E} = \dot{E}_k + \dot{E}_p + \dot{E}_{ph} + \dot{E}_{ch} \quad (3)$$

where \dot{E}_k is kinetic exergy, \dot{E}_p is potential exergy, \dot{E}_{ph} is physical exergy, and \dot{E}_{ch} is chemical exergy. In this research, chemical, kinetic, and potential exergies are neglected; only physical exergy is taken into consideration. Total exergy of a fluid stream can be written as follows (index o refers to the environmental state):

$$\dot{E} = \dot{m}[(h - h_o) - T_o(s - s_o)] \quad (4)$$

The conventional exergy analysis method constructs an exergy equilibrium equation for a specific component in the system and for the entire system. An exergy equilibrium equation for the k -th component in the system is established as follows:

$$\dot{E}_{F_k} = \dot{E}_{P_k} + \dot{E}_{D_k} \quad (5)$$

where \dot{E}_{F_k} is the fuel exergy of the k -th component, \dot{E}_{P_k} is the product exergy of the k -th component, and \dot{E}_{D_k} is the exergy destruction in the k -th component. The fuel exergy of the k -th component is exergetic resource expended to provide product exergy, the product exergy is the desired exergy obtained from the k -th component, and exergy destruction or internal exergy loss is the exergy destroyed due the irreversibility within the k -th component. An exergy equilibrium equation for the system is established as follows:

$$\dot{E}_{F_{tot}} = \dot{E}_{P_{tot}} + \dot{E}_{D_{tot}} + \dot{E}_{L_{tot}} \quad (6)$$

where $\dot{E}_{F_{tot}}$, $\dot{E}_{P_{tot}}$, $\dot{E}_{D_{tot}}$, and $\dot{E}_{L_{tot}}$ represent the fuel exergy, product exergy, exergy destruction, and exergy loss of the overall system, respectively. Exergy loss or external exergy loss is the exergy transfer from the system to its surroundings. The exergy relations used in the conventional exergy analysis for the SORC and DP ORC configurations are given in Appendix A, Table A3, and the exergy relations used in the conventional exergy analysis for the DS parHTSLTPH ORC and DS HTSIHE ORC configurations are given in Table Appendix A, Table A4. The condenser is a dissipative component, since exergy is destroyed without any useful product, and therefore, the equations for the condenser are in parentheses.

2.3. Selected Working Fluids

The most important element in the design process of an ORC plant is certainly working fluid selection. Generally speaking, working fluids used in ORC plants can be classified

into three main categories, i.e., dry, wet and isentropic fluids. Fluids with simple molecular structures behave as wet fluids, while fluids with higher complexity act as the dry fluids. Intermediate fluids belong to isentropic fluids [27]. During the selection process, the environmental factors, such as ozone depletion potential (ODP) and global warming potential (GWP), should be considered, because they contribute to sustainable development. International protocols such as the Montreal Protocol [28], Kyoto Protocol, and Paris Agreement have predicted the substitution of harmful substances that deplete the ozone layer. According to the Montreal Protocol, chlorofluorocarbon (CFC) refrigerants were phased out due to their high ODP and GWP values. Hydrochlorofluorocarbon (HCFC) refrigerants were introduced as substitutes for CFC because they have similar thermodynamic characteristics and having a medium to high GWP and intermediate ODP values. The Montreal Protocol was revised to phase out all HCFCs by 2030. R245fa and R134a represent the most commonly used working fluids in various ORC plants. These working fluids are the most famous representatives of hydrofluorocarbon (HFC) refrigerants. HFCs are third-generation refrigerants and were introduced as transitional substitutes for CFCs and HCFCs. These working fluids have zero ODP, but have high GWP values.

According to the abovementioned information, working fluids that will be used in ORC plants in the future must have zero ODP and low GWP values (lower than 150), and they must achieve good thermodynamic performances in ORC plants. Working fluids that are considered to meet these criteria are HFC with low-GWP, natural refrigerants (carbon dioxide, ammonia, and water), hydrocarbons, and hydrofluoroolefins. Hydrofluoroolefins (HFOs) are environmentally friendly working fluids due to zero ODP and low GWP values. These working fluids are considered to be suitable alternatives to HFC refrigerants [29]. They are mildly flammable, may release hazardous substances, have a high price, and require additional safety requirements [30]. The thermodynamic performance of hydrofluoroolefins as working fluids in ORC plants is still in the research phase [31]. Hydrocarbons (HC) are natural refrigerants that have zero ODP and low GWP values, as well as very good thermodynamic properties [32]. Hydrocarbons provide good compatibility with lubricating oils, they have a low price, and they are highly flammable. Twelve working fluids were selected for research purposes and their basic characteristics are presented in Appendix A, Table A5. Four working fluids were hydrofluoroolefins (R1234yf, R1234ze(Z), R1234ze(E), and R1233zd(E)), while six working fluids were hydrocarbons (cyclopentane, n-pentane (R601), isopentane (R601a), neopentane (R601b), n-butane (R600), and isobutane (R600a)). Hydrochlorofluorocarbon refrigerants R-134a and R-245fa were used for the comparison of the thermodynamic performances predicted by the other hydrocarbons and the hydrofluoroolefins.

2.4. Systems Optimization Procedures

Within the Engineering Equation Solver (EES) software package, a genetic algorithm (GA) was chosen for the optimization process. The specificity of the genetic algorithm (GA) is to reliably locate global optimal values even if the surface has many local peaks, but the process of finding the global optimum is time-consuming. The genetic algorithm has three control operators which need to be selected which are the number of individuals (population), the number of generations, and the maximal mutation rate. The first two control operators are considered to be the most important ones. Before performing calculations, a sensitivity analysis was conducted in order to select the appropriate values for the number of individuals and the number of generations, while the mutation rate was set to 0.2625 in all simulations. For all the optimization calculations, the number of individuals was 100 and the number of generations was 200, as a compromise between the accuracy of the results and computational time.

In this research, different pinch point temperature difference settings are considered as constraints for the optimization. The pinch point temperature difference setting has important consequences on system performance and the cost of the heat exchangers. In the DS HTS IHE ORC configuration, the pinch point temperature difference in the recuperator

or IHE (ΔT_{ppIHE}) is the temperature difference between points 8 and 2 (Figure 2d). This parameter influences the internal heat exchanger (IHE) effectiveness, and also the size of the IHE. For these reasons, the ΔT_{ppIHE} value is limited to 8 °C, which ensures that the IHE effectiveness is large enough with a reasonable IHE size. In the DS parHTS LTPH ORC configuration, the pinch point temperature difference of the low temperature preheater in the HTS was selected to be 10 °C, while, for the LTS preheater, a value of 9 °C was selected. Choosing these values affects the size of the parallel flows of geothermal fluid, but does not affect the net power value of the ORC plant. Optimization of the pinch point temperature difference settings was not considered in this research.

The target of this study is to define the best combination of working fluid(s) and ORC configurations for different low and medium enthalpy geothermal field temperatures (120 °C, 140 °C, 160 °C, and 180 °C). The objective function is the net power output which is maximized for a given geothermal source and ORC configuration. For each ORC configuration, the pinch point temperature differences (model parameters and constraints) are reasonable values assigned which are strictly related to economic considerations. For the SORC independent variables, cycle maximum pressure and superheating temperature difference were selected. In all simulations, the bounds for superheating temperature differences were from 5 °C to 20 °C. For cycle maximal pressure, the bounds were separately determined by parametric analysis for each working fluid. For the dual-pressure ORC (DP ORC), the independent variables were high pressure, low pressure, high-pressure superheating temperature difference, and low-pressure superheating temperature difference. The bounds for cycle high pressure and low pressure were separately determined by parametric analysis for each working fluid. For the DS parHTSLTPH ORC, the independent variables were HTS pressure, LTS pressure, HTS superheating temperature difference, and LTS superheating temperature difference. The bounds for HTS pressure and LTS pressure were separately determined by parametric analysis for each working fluid. For the DS HTSIHE ORC, the independent variables were HTS pressure, LTS pressure, HTS maximum temperature, and LTS superheating temperature difference. The bounds for HTS pressure and LTS pressure were separately determined by parametric analysis for each working fluid.

3. Results and Discussion

3.1. Thermodynamic Optimization Proposed ORC Configurations

The selected ORC configuration performances are optimized for maximum net power output. Some important results obtained from the optimization runs are shown in this section. The results for the SORC configuration are shown in Figure 3 and Appendix A, Table A5.

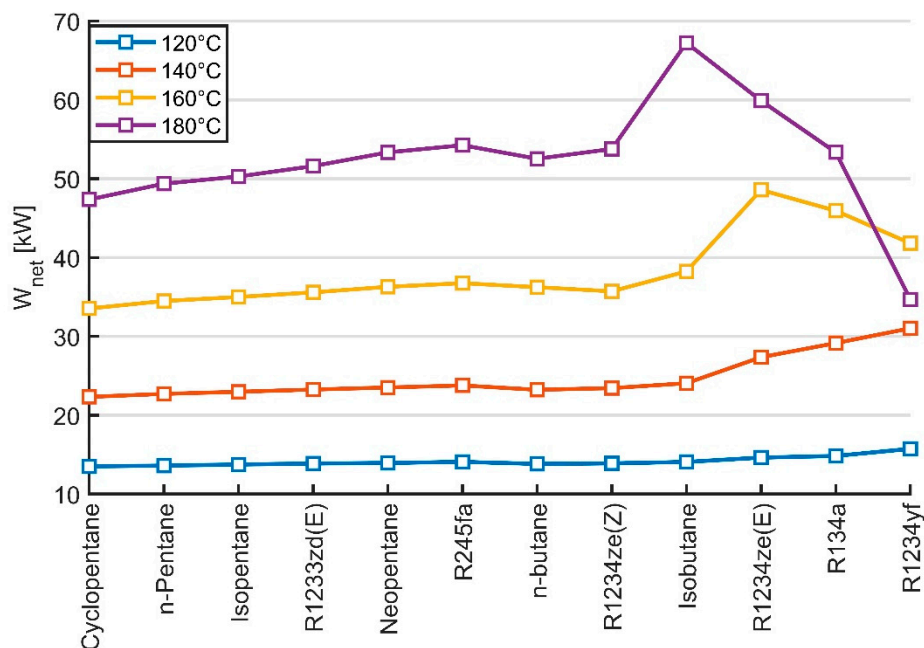


Figure 3. The net power output of the SORC configuration, as a function of the working fluids, for the geothermal heat source characteristic temperatures.

The highest values of net power at temperatures of 120 °C and 140 °C are achieved with the working fluid R1234yf, namely 15.74 and 31.07 kW. At geothermal temperatures of 160 °C and 180 °C, the best results are achieved by the working fluids R1234ze(E) and isobutane with a net power of 48.58 kW and 67.23 kW, respectively. Thus, the highest values of net power are achieved by working fluids that have a critical temperature value from 25.3 °C to 50.6 °C lower than the geothermal fluid temperature. Similar results were achieved for the DP ORC configuration, which are shown in Appendix A, Table A6 and in Figure 4. At lower geothermal fluid temperature values (120 °C and 140 °C), the highest net power is realized with R1234yf, with values of 18.58 kW and 31.07 kW, respectively. At a geothermal fluid temperature of 160 °C, the highest net power is generated with isobutene (50.0 kW), while at 180 °C, n-butane achieves the best performance with 69.67 kW. Similar to the previous ORC configuration, the highest values of net power were achieved by working fluids whose critical temperature values are from 25.3 °C to 30.6 °C lower than the inlet temperature of the geothermal fluid. It is interesting to note that when comparing the SORC and DP ORC configurations, the greatest increase in net power is achieved with working fluids with the highest value of critical temperature (cyclopentane). The indicated increase in net power decreases as the geothermal fluid temperature increases, and the magnitude of the critical temperature of the working fluid decreases. For example, the working fluid R1234yf, which achieves the highest net power values at lower values of the geothermal fluid temperatures, achieves a very small increase in net power at 120 °C, while at a temperature of 140 °C it achieves a negative increase.

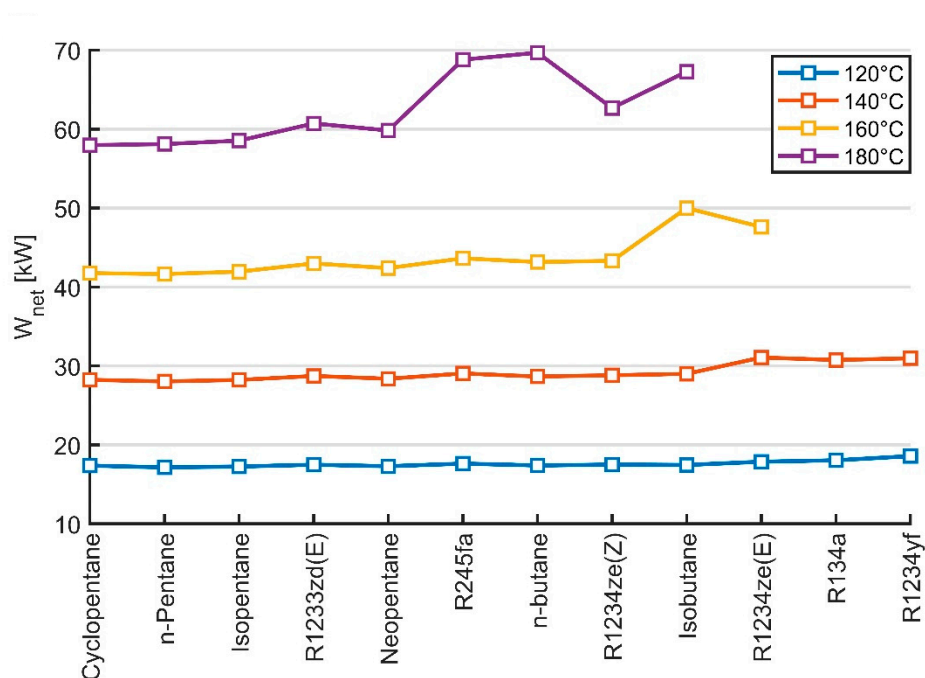


Figure 4. The net power output of the DP ORC configuration, as a function of the working fluids, for the geothermal heat source characteristic temperatures.

The net power output of the DS parHTSLTPH ORC configuration, as a function of the working fluids in the HTS and LTS stages, for the geothermal heat source characteristic temperatures is shown in the Figure 5. For this ORC configuration, 144 combinations of working fluids were optimized for each geothermal heat source characteristic temperature. In Figure 5, the values of the net power for the geothermal fluid temperature of 120 °C are presented. In general, it can be observed that there is a relatively small difference in the optimal net power output of the corresponding ORC configurations which have different working fluids in the HTS and the LTS, especially with working fluids in the HTS whose critical temperature values are much higher than the geothermal fluid temperature. The value of net power tends to increase more significantly in configurations with working fluids in the HTS whose value of critical temperatures is lower than the geothermal fluid temperature. Furthermore, there are only relatively small deviations in the value of the net power between the configurations in which the same working fluid is used in the HTS. The value of the net power (mainly) increases slightly from the working fluids in the LTS with the highest values, to the working fluids with the lowest values of the critical temperature. The configuration with R1234yf working fluid in the HTS, which has a lower critical temperature value than all considered working fluids, achieves the highest values of net power. The highest value of net power of 18.51 (kW) was achieved by the configuration with R1234yf in the HTS and the LTS. Approximately 85% of the net power is realized in the HTS, while the remaining 15% is realized in the LTS. At a geothermal fluid temperature of 140 °C, a similar pattern of realized values of net power occurs, as shown in Figure 6. The maximum net power values appear in configurations where the working fluid in the HTS is R1234ze(E). The DS parHTSLTPH ORC configuration with a combination of working fluids R1234ze(E)/R1234yf (HTS/LTS) achieves the highest value of net power in the amount of 30.96 kW. With an increase in the geothermal fluid temperature (from 160 °C to 180 °C), the pattern net power values of ORC configurations changes significantly, as shown in Figure 3. At 160 °C, the highest values of net power are achieved by configurations with isobutane in the HTS, while at 180 °C, the highest values of net power are achieved by configurations with R1234ze(Z) and R245fa (slightly lower values) in the HTS. From the analyzed results, it can be concluded that the highest values of net power are achieved by configurations whose working fluids in the HTS have a critical temperature value that is

from 25 °C to 30 °C lower than the geothermal fluid temperature. At higher geothermal fluid temperatures of 120 °C, not all working fluids are taken into consideration. The reason for this is that these working fluids, which have the lowest values of critical temperatures, at characteristic temperatures give a solution where the net power of the LTS is represented in the amount of less than 1 to 2%.

In Figure 6, the net power of the DS HTSIHE ORC configuration, for the geothermal heat source characteristic temperatures, is shown as a function of the working fluids in the HTS and the LTS. In total, 144 combinations of working fluids are optimized for geothermal heat source temperatures from 120 °C to 160 °C, except at 180 °C where the working fluids R1234ze(E), R134a, and R1234yf are not included in the consideration. From the analysis of the results shown in Figure 6, it can be concluded that, for geothermal fluid temperatures from 120 °C to 160 °C, the change pattern of net power values of the ORC configurations is similar. The ORC configurations with working fluids in the HTS whose critical temperature values are much higher than the geothermal fluid temperature have relatively small differences in the optimal net power output. The value of net power increases more significantly in the ORC configurations with working fluids in the HTS whose value of critical temperatures is lower than the geothermal fluid temperature, and the highest values of net power are achieved by ORC configurations whose working fluids in the HTS have critical temperature values that are from 25.3 °C to 50.6 °C lower than the geothermal fluid temperature. For the ORC configurations with the same working fluid in the HTS, relatively small deviations appear in the net power values, which increase slightly from the working fluids in the LTS with the highest values, to the working fluids with the lowest values of the critical temperature. At a geothermal fluid temperature of 180 °C, all net power values are quite similar, except in a narrow area where they reach maximum values. The ORC configurations with R1234yf in the HTS achieve the highest values of net power at 120 °C; at 140 °C, these are the ORC configurations with R134a; at 160 °C, these are ORC configurations with R1234ze(E); while at 180 °C, these are ORC configurations with isobutane.

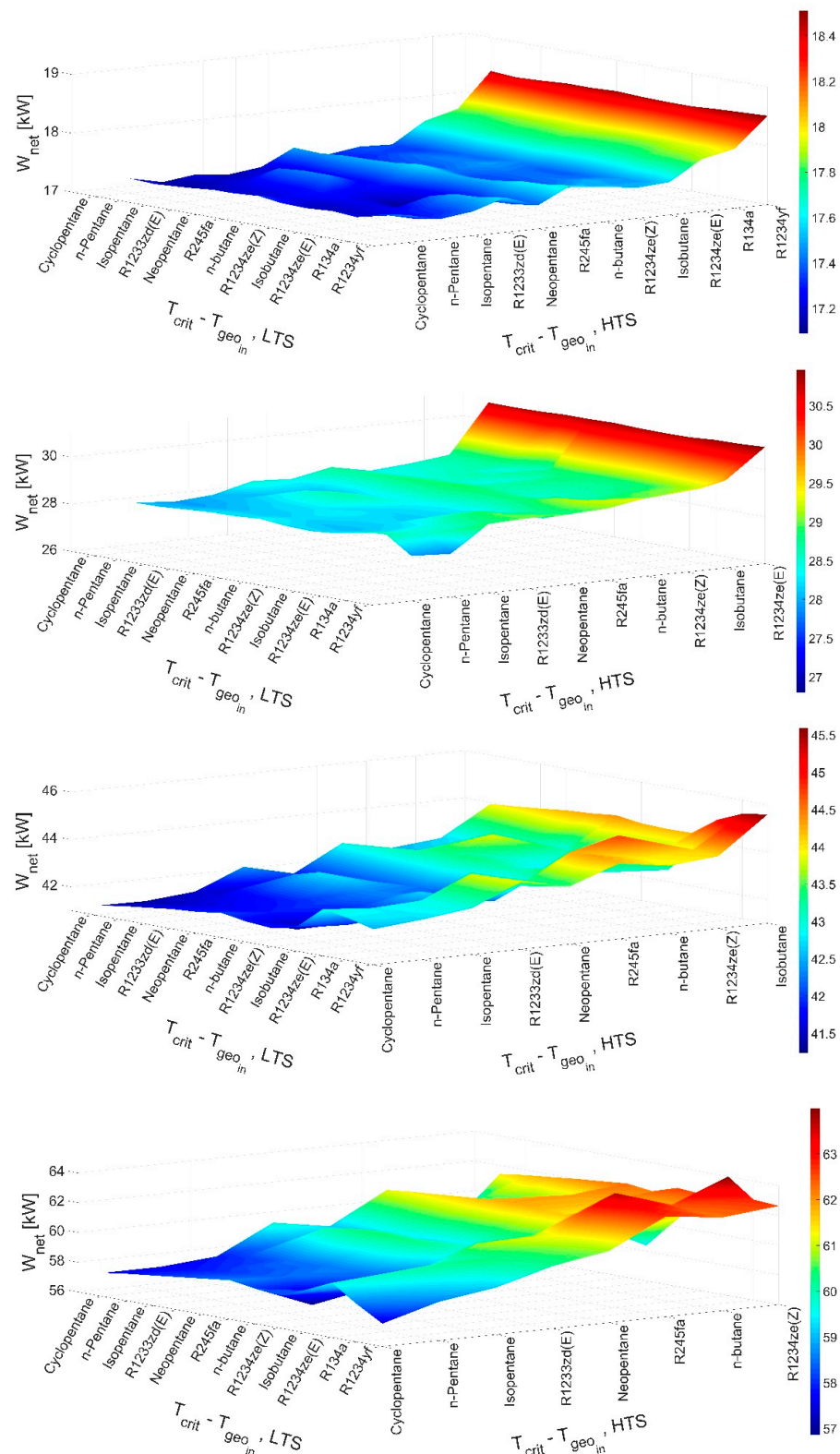


Figure 5. The net power output of the DS parHTSLTPH ORC configuration, as a function of the working fluids in the HTS and the LTS, for the geothermal heat source characteristic temperatures.

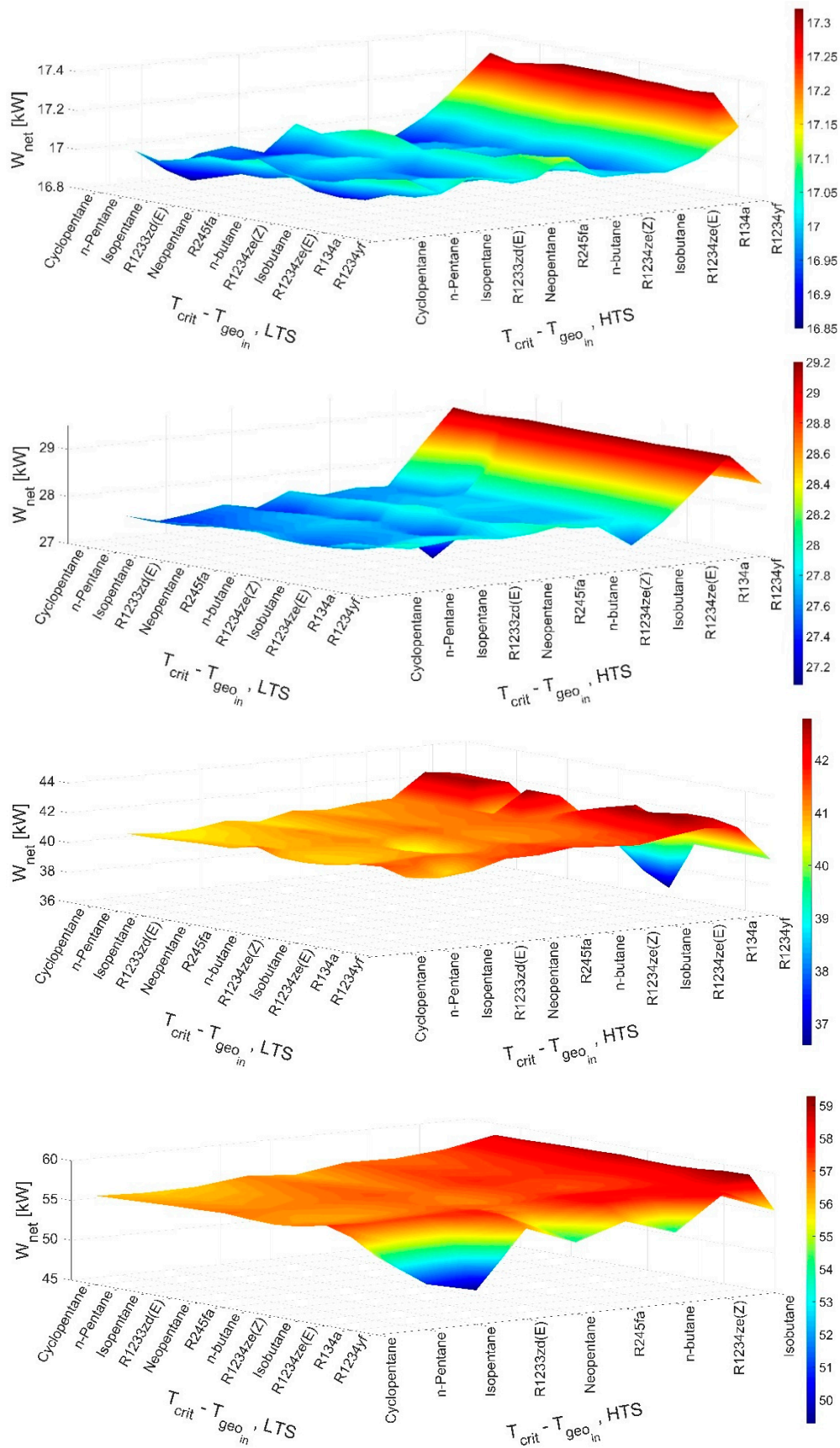


Figure 6. Net power output of the DS HTSIHE ORC configuration, as a function of the working fluids in HTS and the LTS, for the geothermal heat source characteristic temperatures.

One of the goals of this research is to determine how much the net power increases (or decreases) in selected configurations as compared with the SORC configuration under the same thermodynamic conditions. Therefore, the value of the SORC net power for the corresponding working fluid was compared with the value of the net power of the considered DS configuration with the same working fluid in the HTS. The obtained results are shown in Figure 7 for the DS parHTSLTPH ORC, and in Figure 8, for the DS HTSIHE ORC configuration. In the case of DS parHTSLTPH ORC (Figure 7), in general it can be concluded that there is an increase in net power as compared with the SORC configuration, but the size of the increase in net power depends on the geothermal fluid temperature and the type of working fluid in the ORC configuration. The size of the increase in net power depends solely on the type of working fluid in the HTS. At 120 °C, the greatest increase in net power is achieved with cyclopentane, and the smallest increase in net power occurs with R1234yf. At 140 °C, the configurations with cyclopentane, isopentane, and n-butane achieve the greatest increases in net power. At 160 °C and 180 °C, the values of net power increases are uniform, ranging from 7 kW to 9 kW (at 160 °C) and from 8 kW to 10 kW (at 180 °C); a significant increase for isobutanes (at 160 °C); and a significant drop in net power values for n-butanes at a geothermal fluid temperature of 180 °C. In the case of DS HTSIHE ORC (Figure 8), in general, it is also possible to conclude that there is an increase in net power (mostly) as compared with the SORC configuration, but the size of the increase in net power depends on the geothermal fluid temperature and the type of working fluid in the ORC configurations. The size of the increase in net power depends solely on the type of working fluid in the HTS. At lower values of geothermal fluid temperatures (120 °C and 140 °C), a similar trend of increased net power values can be observed where cyclopentane achieves the highest values, while R1234yf has a negative increase in net power. At 160 °C, there are uniform values of net power increase ranging from 4 kW to 8 kW; and R1234ze(E), R134a, and R1234yf have negative values of net power increase. At 180 °C, cyclopentane again achieves the largest increase in net power value, while isobutane is the only one to record a negative value of net power increase.

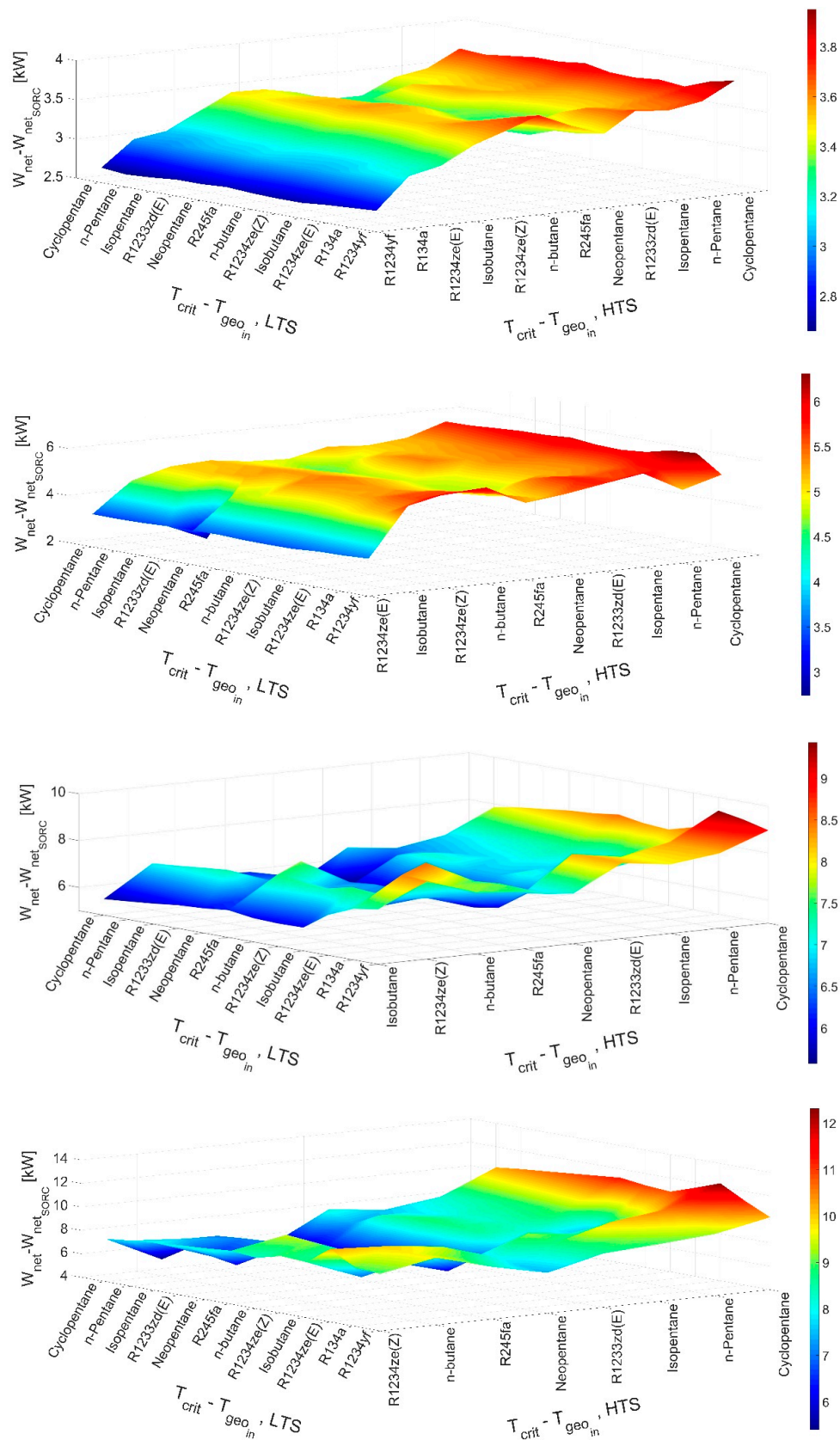


Figure 7. Net power values of the DS parHTSLTPH ORC configuration as compared with the SORC configuration for the corresponding working fluids in the HTS.

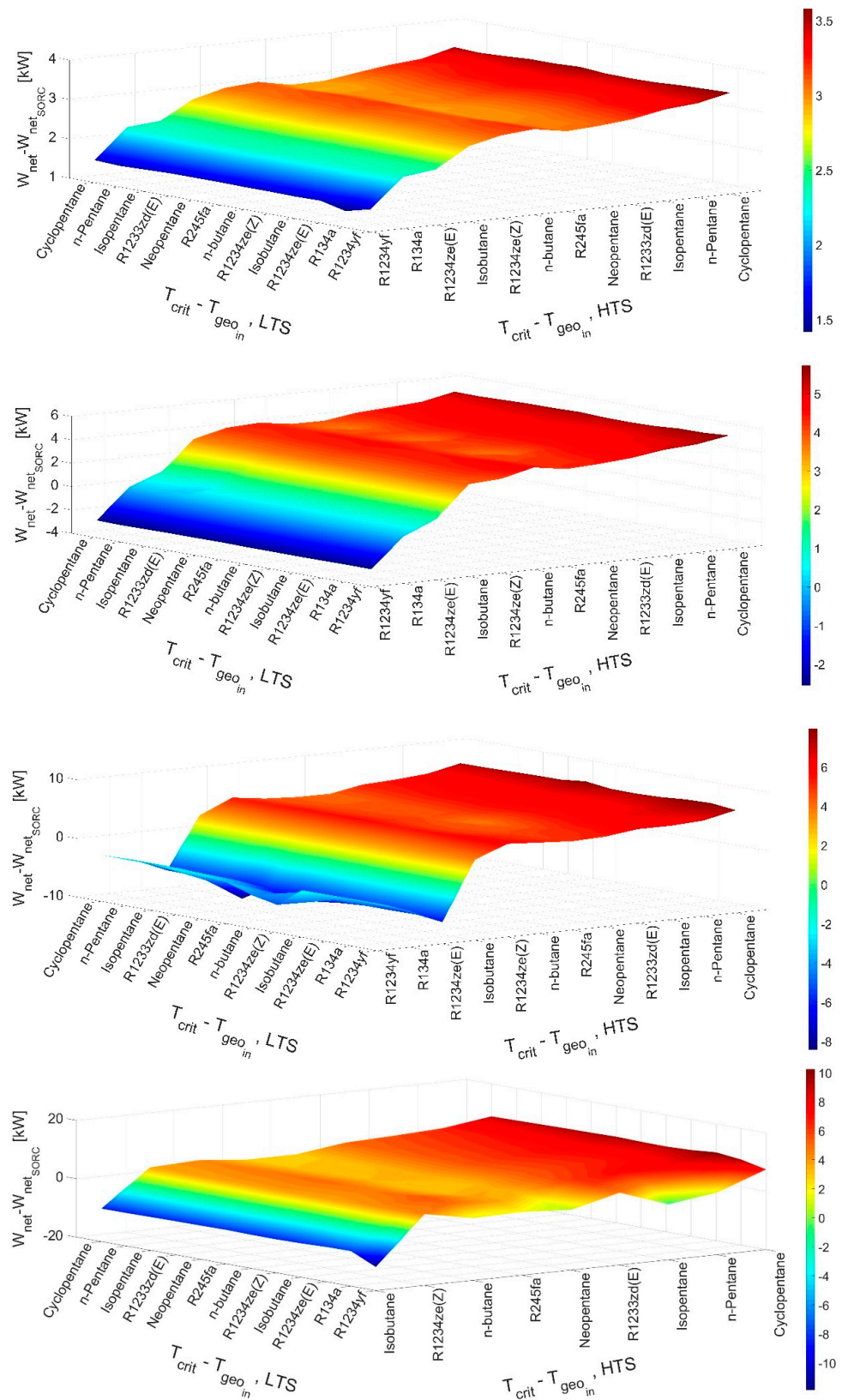


Figure 8. Net power values of the DS HTSIHE ORC configuration as compared with the SORC configuration for the corresponding working fluids in the HTS.

The thermodynamic states of the working fluids, geothermal fluid (water), and cooling fluid (air) in characteristic points of the DS ORC configurations with R1234yf in the HTS

and the LTS for a geothermal fluid temperature of 120 °C are presented in Appendix A, Table A7 (for the DS parHTSLTPH ORC configuration) and Appendix A, Table A8 (for the DS HTSIHE ORC configuration).

3.2. Analysis of Thermodynamic Optimization Results

Figure 9 shows the best representatives of individual ORC configurations that achieve the highest values of net power at characteristic temperatures of the geothermal fluid. At a geothermal fluid temperature of 120 °C, the highest value of net power (18.58 kW) was achieved by the DP ORC configuration, followed by the DS parHTSLTPH ORC configuration (18.51 kW), and the DS HTSIHE ORC configuration (17.32 kW). The lowest value of net power was realized by the SORC configuration (15.74 kW). It should be noted, in the case of the DP ORC configuration, that 71% of the work was realized in the low-pressure turbine, while, in the case of the DS parHTSLTPH ORC configuration, 84.7% of the net power was generated in the HTS. In all mentioned ORC configurations, the working fluid was R1234yf (in the HTS and the LTS in the DS ORC configuration). At a geothermal fluid temperature of 140 °C, all the considered ORC configurations achieved similar values of net power. The DP ORC configuration achieved a net power of 31.07 kW with working fluid R1234ze(E), the SORC configuration achieved a net power of 31.03 kW with working fluid R1234yf, the DS parHTSLTPH ORC configuration with a combination of working fluids R1234ze(E)/R1234yf (HTS/LTS) achieved a net power of 30.96 kW, while the DS HTSIHE ORC configuration with a combination of working fluids R134a/R134a (HTS/LTS) achieved a net power of 29.2 kW. The characteristic of the double stage (DS) configurations is that most of the net power is realized in the HTS, and therefore, in the DS parHTSLTPH ORC configuration, 11.85% of the net power, while in the DS HTSIHE ORC configuration, 11.99% of the net power is realized in the LTS. It should be noted, in the case of the DS HTSIHE ORC configuration, that the same highest value of net power (29.2 kW) is achieved by the combination of working fluids R134a/R1234yf (HTS/LTS). In the case of the mentioned ORC configuration, the best performance in the category of low GWP working fluids is achieved by the R1234ze(E)/R1234yf (HTS/LTS) combination, where a net power value of 28.58 kW is realized. By increasing the temperature of the geothermal fluid to 160 °C, as well as to 180 °C, the same order appears of ORC configurations realized net powers. The most net power is produced in the DP ORC configuration, namely 50.0 kW (at 160 °C) with isobutane and 69.67 kW (at 180 °C) with n-butane. The SORC configuration achieves slightly lower values of net power in the amount of 48.58 kW at 160 °C with R1234ze(E), and at 180 °C, it achieves 67.23 kW with isobutane as working fluid. A somewhat lower value of net power is produced in the DS parHTSLTPH ORC configuration, while the DS HTSIHE ORC configuration produces the lowest net power values. At a geothermal fluid temperature of 160 °C, the DS parHTSLTPH ORC configuration achieves 45.59 kW of net power with the isobutane/R1234yf working fluid combination, of which 21.68% is realized in the LTS. The trend of increasing the share of net power in the LTS continues at 180 °C, where, of the produced 63.99 kW with R1234ze(Z)/R1234ze(Z), 24.1% is realized in the LTS. The combination of working fluids R1234ze(E)/R134a in the DS HTSIHE ORC configuration achieves a net power of 42.78 kW at a geothermal fluid temperature of 160 °C, while at 180 °C with the combination of working fluids isobutane/R134a, it produces 59.28 kW. However, the share of work in the LTS increases from 11.98% at 160 °C to 19.21% at 180 °C.

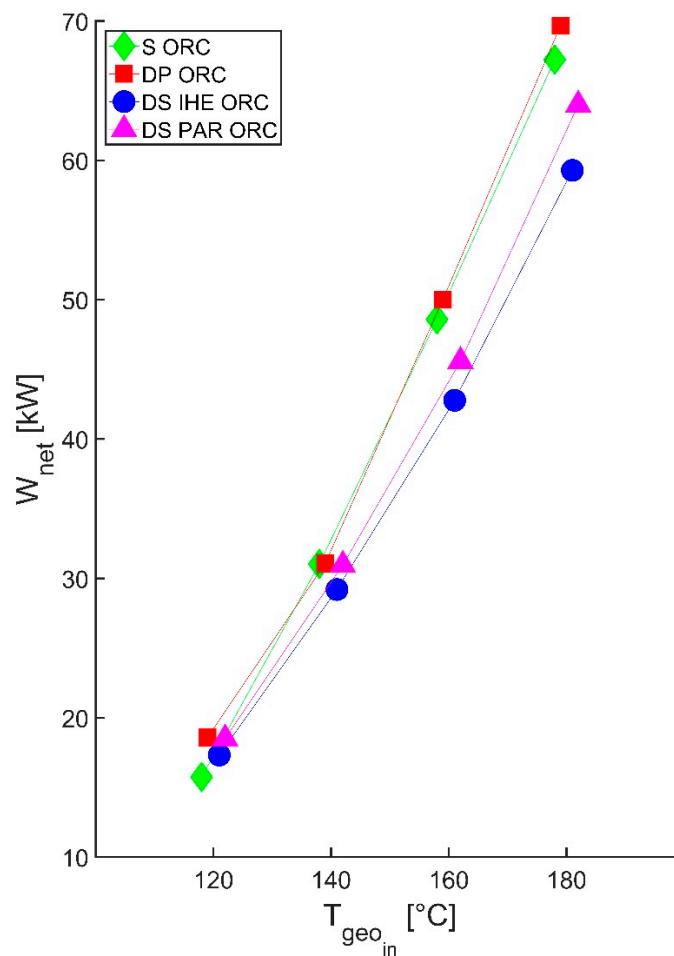


Figure 9. The best representatives of the individual ORC configurations that achieve the highest values of net power at characteristic temperatures of the geothermal fluid.

It has been established in the scientific literature [26] that DP ORC configurations do not provide any significant gain in net power as compared with the SORC configuration when the critical temperature of the working fluid is approximately 40 °C lower than the heat source inlet temperature, which corresponds to the optimality criterion of the SORC configuration that $T_{cr} \approx T_{geo_in} - 40$ °C (T_{cr} is the critical temperature and T_{geo_in} is the inlet temperature of the geothermal fluid). The results obtained for the SORC and DP ORC configurations, which are given in Tables A6 and A7 (in Appendix A) and Figures 3 and 4, fully confirm the stated optimality criterion. The question arises whether the mentioned optimality criterion is valid after the given DS ORC configuration? Therefore, it is necessary to define the dependence between the geothermal fluid temperature, the critical temperatures of the working fluids used in the DS ORC stages, and the improvement potential of the thermodynamic performance (net power), by analyzing the data shown in Figure 7 for the DS parHTSLTPH ORC configuration, and in Figure 8 for the DS HTSIHE ORC configuration. The analysis of the data for the DS parHTSLTPH ORC configuration indicates that, due to the limited set of given working fluids, we cannot accurately determine the value of the optimality criterion for the SORC configuration, but it can be claimed that it is greater than 30 °C. For the DS HTSIHE ORC configuration, the value of the optimality criterion for the SORC configuration can be relatively accurately determined, and its value ranges between 39 °C and 45 °C. Due to the previously stated facts, the value of the temperature difference between the inlet temperature of the geothermal fluid and the critical temperature of the working fluid in the HTS (hereinafter the term temperature difference will be used) represents very important information, which we will use to analyze the

obtained results. At a geothermal fluid temperature of 120 °C, the working fluids in all the best representatives of the individual ORC configurations is R1234yf. For the SORC configuration, the temperature difference is 25.3 °C, as well as the temperature difference for the other considered ORC configurations. That temperature difference value means that the SORC configuration did not meet the optimality criterion, because the value must be greater than 40 °C. Since all the ORC configurations use the same working fluid, this means that the DP ORC configuration, as well as the other two DS ORC configurations, achieve a higher net power value than the SORC configuration. The net power value of the SORC configuration could be increased if a working fluid with a significantly lower critical temperature value was available. At a geothermal fluid temperature of 120 °C, the best representatives of individual ORC configurations achieve the following temperature differences: SORC 45.3 °C (R1234yf), DP ORC 30.6 °C (R1234ze(E)), DS HTSIHE ORC 39.0 °C ((R134a/R134a) and DS parHTSLTPH ORC 30.6 °C (R1234ze(E)/R1234yf). The ORC configurations all have temperature difference values at the limit values of the optimality criterion, which has the consequence that the net power values are similar. The same logic can be applied to analyze the results obtained at geothermal fluid temperatures of 160 °C and 180 °C.

3.3. Conventional Exergy Analysis

A conventional exergy analysis was performed on representatives of all the considered ORC configurations that achieved the highest value of net power for a given geothermal fluid temperature.

The results of the conventional exergy analysis are presented in Figure 10. The results for four considered ORC configuration representatives at a geothermal fluid temperature of 120 °C. Based on the obtained results, it can be seen that the highest exergy losses were realized in the SORC configuration, followed by the DS HTSIHE ORC configuration, while the lowest exergy losses were in the DS parHTSLTPH ORC and DP ORC configurations. In both ORC configurations (SORC and DS HTSIHE ORC), the lower values of net power achieved were due to the fact that exergy losses were the highest. It should be noted that these two ORC configurations achieved the lowest values of total exergy destruction; however, the amount of loss was still too large, and therefore, the net power values achieved were still the lowest. In all the ORC configurations, the greatest destruction of exergy occurred in different heat exchangers, during heat removal from the cycle with air in an air-cooled condenser (desuperheater, especially condenser and subcooler), and during heat absorption heat from the geothermal fluid (preheater, evaporator, and superheat). The two ORC configurations that achieved the highest net power values at a geothermal fluid temperature of 120 °C were the DP ORC and DC parHTSLTPH ORC configurations. These ORC configurations achieved approximately the same values of exergy losses and exergy destruction rates. In general, it can be concluded that at all geothermal fluid temperatures, except 120 °C, the DS HTSIHE ORC configuration achieved the highest values of exergy losses and exergy destruction rates in heat exchangers that supply heat to the cycle from the geothermal fluid. At a geothermal fluid temperature of 140 °C, all the ORC configurations (except DSHTSIHE ORC) achieved similar values of the total sum of exergy losses and exergy destruction. The SORC configuration had the highest value of the sum of exergy destruction rates, the highest exergy destruction in the pumps was achieved in the DP ORC configuration, while the highest exergy destruction in the turbines was achieved by the DS HTSLTPH ORC configuration. At higher geothermal fluid temperatures (160 °C and 180 °C) the lowest value of the total sum of exergy losses and exergy destruction rates were achieved by the DP ORC configuration, which was followed by the SORC configuration with slightly higher values. The DP ORC configuration achieved higher values of exergy losses, while the SORC configuration had a higher value of exergy destruction in heat exchangers that supplied heat to the cycle from the geothermal fluid.

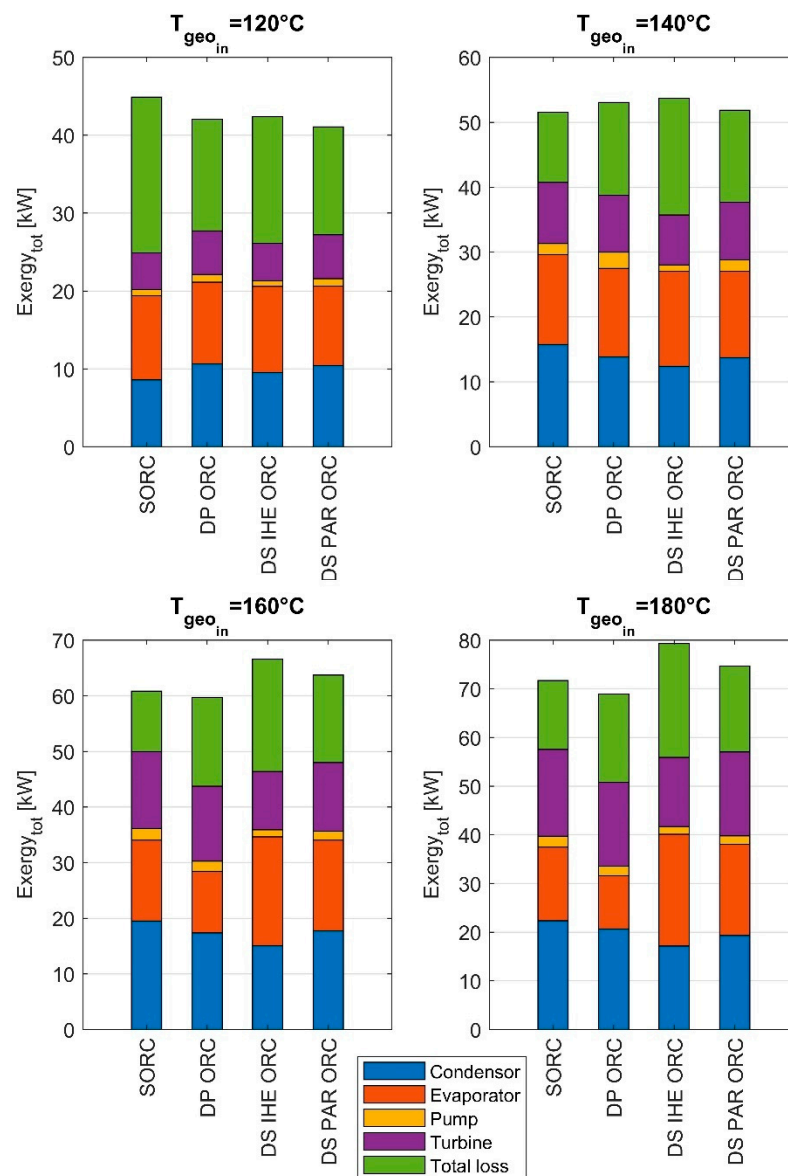


Figure 10. The results of the conventional exergy analysis.

3.4. Indirect Economic Indicators Analysis

Indirect economic indicators do not directly measure the economics of the entire ORC configuration, but can qualitatively characterize the cost of some plant components. The intention is to use selected simple indirect economic indicators to indicate whether the best representatives of individual ORC configurations that achieve the superior thermodynamic characteristics have equally good techno-economic characteristics. The selected indirect economic indicators are total thermal conductance value (AU_{tot}) for heat exchangers [33] and net power to total thermal conductance ratio (W_{net} / AU_{tot}).

The thermal conductance of the k -th heat exchanger (UA_k) is proportional to its size, and could be considered to represent the initial cost of the heat exchanger. Thermal conductance can be calculated from basic thermodynamic data and represents the ratio of the exchanged heat in the heat exchanger and the mean logarithmic temperature difference. The total thermal conductance (AU_{tot}) value for a particular ORC configuration is obtained by adding all the thermal conductance values of individual heat exchangers in a configuration. Figure 11a shows the values of total thermal conductance for the best representative ORC configurations depending on the temperature of the geothermal fluid.

At a geothermal fluid temperature of 120 °C, the lowest value of total thermal conductance (AU_{tot}) is achieved by the SORC configuration, while the highest value is achieved by the DP ORC configuration; the AU_{tot} value of the DP ORC configuration is 67% higher than that of the SORC configuration. The DSparHTSLTPH ORC and DS HTSIHE ORC configurations achieve AU_{tot} values that are approximately 24% and 25% higher than that of the SORC configuration. If we compare the thermal conductance values for the DP ORC and DS parHTSLTPH ORC configurations, which achieve approximate values of net power at 120 °C, then we see that the DP ORC configuration has a significantly higher thermal conductance value of the heat exchangers for exchange heat from the geothermal fluid (28.0 versus 17.54 (kW/K)), while the values for the condensers are approximately the same. Thermal conductance values for all the considered geothermal fluid temperatures for the DS HTSIHE ORC and DS parHTSLTPH ORC configurations achieve similar values and increase linearly with temperature. An identical trend of linear increase in the thermal conductance value with geothermal fluid temperature is achieved by the DP ORC configuration, but with higher values than the previous two ORC configurations. The SORC configuration realizes a rush linear growth of the thermal conductance value up to the geothermal fluid temperature of 160 °C, when it reaches the maximum value, which is the highest of all the ORC configurations. This is followed by a drop in the thermal conductance value, and at 180 °C, it achieves a slightly lower value than the DP ORC configuration. Figure 11b shows the comparison of $AU_{tot}/AU_{tot-SORC}$ values for the considered configurations. It should be emphasized that at higher geothermal fluid temperatures (from 140 °C to 180 °C), double stage (DS) ORC configurations achieve lower thermal conductance values than the SORC and DP ORC configurations.

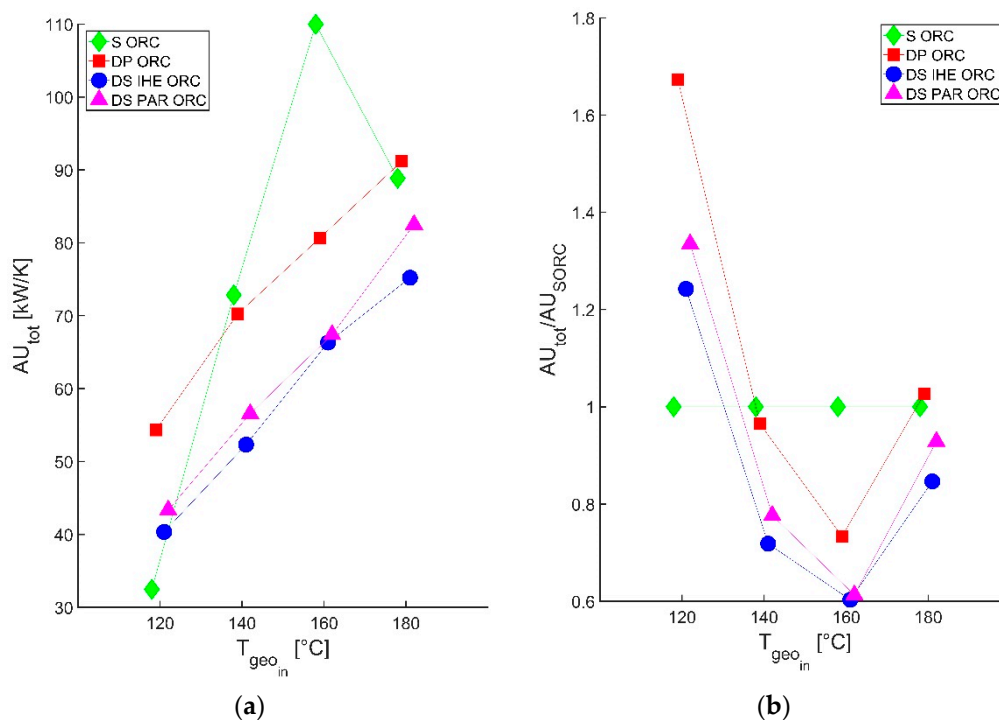


Figure 11. (a) The comparison of AU_{tot} values of individual ORC configurations with the SORC configuration values, at different geothermal fluid temperatures; (b) the comparison of $AU_{tot}/AU_{tot-SORC}$ values for the considered configurations.

The ratio of the net power to the total thermal conductance (W_{net}/AU_{tot}) of an ORC configuration can be interpreted as the ratio of the system earning and system cost, and can be used as a preliminary indirect economic indicator. Figure 12 shows the comparison of the specified indirect economic indicator values (W_{net}/AU_{tot}) for the other ORC confi-

urations versus indicator values for the SORC configuration ($W_{net-SORC}/AU_{tot-SORC}$), at the considered temperatures of the geothermal fluid. At 120 °C, the SORC configuration achieves the highest value of the indicator, while at 140 °C and 160 °C, the double stage (DS) configuration has the highest value of the indicator. At a geothermal fluid temperature of 180 °C, all the ORC configurations achieve a similar indicator value. The obtained results point to the necessity of including economic analysis and optimization in the process of selecting the most suitable ORC configuration and working fluids for particular geothermal fluid temperatures.

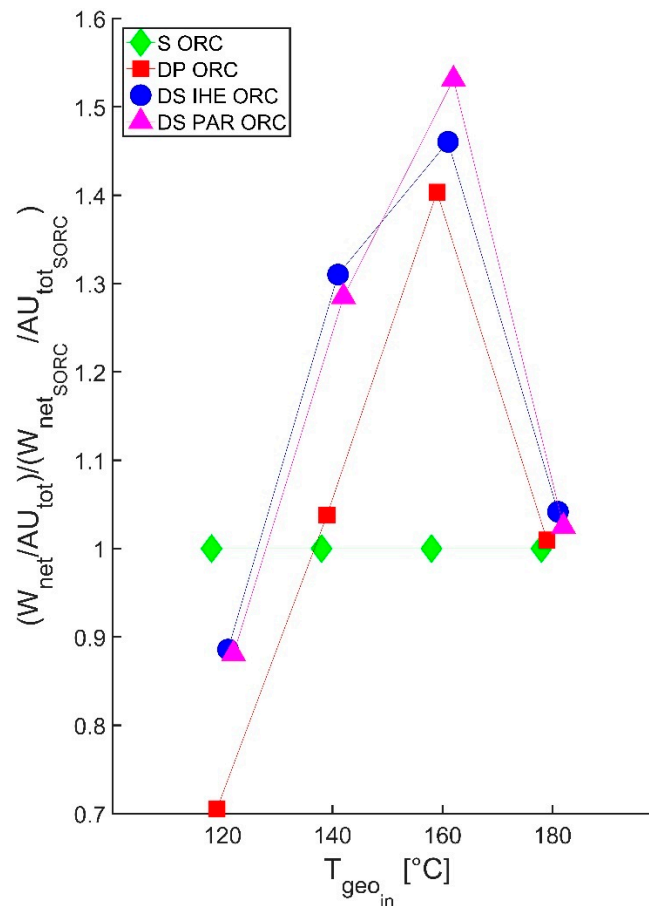


Figure 12. The comparison of $(W_{net}/AU_{tot})/(W_{net-SORC}/AU_{tot-SORC})$ values for the considered configurations.

4. Conclusions

This study has explored the real potential of selected advanced Organic Rankine Cycle configurations in improving the thermodynamic performance of the simple ORC (SORC) for low and medium enthalpy geothermal fields that have temperatures from 120 °C to 180 °C with the application low global warming potential working fluids. The considered advanced Organic Rankine Cycle configurations are: dual-pressure ORC (DP ORC), double stage serial-parallel ORC configuration with a low-temperature preheater in a high-temperature stage ORC (DS parHTS LTPH ORC), and serial double stage ORC with internal heat exchanger in high-temperature stage ORC (DS HTSIHE ORC). The selected Organic Rankine Cycle configurations were all optimized using the net power output as the objective function. An extensive evaluation of the obtained results made it possible to draw the following general conclusions.

Working fluids with a low GWP value show excellent thermodynamic characteristics that depend on the geothermal fluid temperature and the magnitude of the critical temperature.

The DP ORC and DS parHTSLTPH ORC configurations, depending on the geothermal fluid temperature, and with the use of the appropriate working fluid(s), achieve very good thermodynamic characteristics, and therefore, are recommended for use in commercial engineering applications in future. For the DS HTSIHE ORC configuration (and similar configurations), it is necessary to carry out further analyses because it achieves high values of the corresponding indirect economic indicators.

Earlier research has confirmed that there is an optimality criterion of the SORC configuration with regard to the DP ORC configuration. In this work, it is determined that a similar optimality criterion of the SORC configuration exists for the DS HTSIHE ORC configuration and the DS parHTSLTPH ORC configuration (partially identified).

It can be concluded that extensive thermo-economic studies should be carried out to assess the competitiveness of the considered advanced ORC configurations, since they may be associated with significantly increased equipment costs.

Author Contributions: N.M., conceptualization, creation of the idea, selected ORC configuration performances and optimization for maximum net power output, writing, reviewing, and editing of the whole manuscript; V.B., preparation of the data presented in the paper and writing the discussion and conclusion; Ž.D., preparation of the geothermal field data (temperatures) for the ORC configuration performances, preparation of the figures; T.K., preparation of tables and figures, preparation of the comprehensive literature overview visualization, writing the results. All authors have read and agreed to the published version of the manuscript.

Funding: This research received no external funding.

Institutional Review Board Statement: Not applicable.

Informed Consent Statement: Not applicable.

Data Availability Statement: Data available in a publicly accessible repository.

Conflicts of Interest: The authors declare no conflict of interest.

Nomenclature

| | | |
|------------------|------------------------|----------|
| h | Specific enthalpy | [kJ/kg] |
| \dot{m} | Mass flow rate | [kg/s] |
| \dot{W} | Work flow rate power | [kW] |
| \dot{Q} | Heat flow rate | [kW] |
| \dot{E} | Exergy | [kW] |
| s | Specific entropy | [kJ/kg] |
| T | Temperature | [°C] |
| AU | Thermal conductance | [kW/K] |
| c_p | Specific heat capacity | [kJ/kgK] |
| P | Pressure | [bar] |
| Greek symbols | | |
| η | Thermal efficiency | [%] |
| ΔT | Temperature difference | [°C] |
| $\Delta \dot{W}$ | Work rate difference | [kW] |

Appendix A

Table A1. The relations for each component (first law analysis) for the SORC and DP ORC configurations.

| Configuration Component | SORC | DP ORC |
|-------------------------|---|--|
| Pump | $\eta_p = \frac{h_{2s} - h_1}{h_2 - h_{10}}$ $\dot{W}_p = \frac{\dot{m}_{wf} \cdot (h_2 - h_1)}{\eta_{m,p}}$ | $\eta_{p,LP} = \frac{h_{2s} - h_1}{h_2 - h_1}$ $\dot{W}_{p,LTS} = \frac{\dot{m}_{wf} \cdot (h_2 - h_1)}{\eta_{m,p}}$ $\eta_{p,HP} = \frac{h_{4s} - h_3}{h_4 - h_3}$ $\dot{W}_{p,HP} = \frac{\dot{m}_{wf,HP} \cdot (h_4 - h_3)}{\eta_{m,p}}$ |
| Preheater | $\dot{Q}_{PH} = \dot{m}_{wf} \cdot (h_3 - h_2)$ $\dot{Q}_{PH} = \dot{m}_{geo} \cdot c_{p,geo1} \cdot (T_{11} - T_{12})$ | $\dot{Q}_{PH,LP} = \dot{m}_{wf} \cdot (h_3 - h_2)$ $\dot{Q}_{PH,LP} = \dot{m}_{geo} \cdot c_{p,geo6} \cdot (T_{20} - T_{21})$ $\dot{Q}_{PH,LP} = \dot{m}_{wf,HP} \cdot (h_5 - h_4)$ $\dot{Q}_{PH,HP} = \dot{m}_{geo} \cdot c_{p,geo3,PH,HP} \cdot (T_{17} - T_{18})$ |
| Evaporator | $\dot{Q}_{EV} = \dot{m}_{wf} \cdot (h_4 - h_8)$ $\dot{Q}_{EV} = \dot{m}_{geo} \cdot c_{p,geo2} \cdot (T_{10} - T_{11})$ | $\dot{Q}_{EV,LP} = \dot{m}_{wf,LP} \cdot (h_9 - h_3)$ $\dot{Q}_{EV,LP} = \dot{m}_{geo} \cdot c_{p,geo5} \cdot (T_{19} - T_{20})$ $\dot{Q}_{EV,HP} = \dot{m}_{wf,HP} \cdot (h_6 - h_5)$ $\dot{Q}_{EV,HP} = \dot{m}_{geo} \cdot c_{p,geo2} \cdot (T_{16} - T_{17})$ |
| Superheater | $\dot{Q}_{SH} = \dot{m}_{wf} \cdot (h_5 - h_4)$ $\dot{Q}_{SH} = \dot{m}_{geo} \cdot c_{p,geo3} \cdot (T_9 - T_{10})$ | $\dot{Q}_{SH,LP} = \dot{m}_{wf,LP} \cdot (h_{10} - h_9)$ $\dot{Q}_{SH,LP} = \dot{m}_{geo} \cdot c_{p,geo4} \cdot (T_{18} - T_{19})$ $\dot{Q}_{SH,HP} = \dot{m}_{wf,HP} \cdot (h_7 - h_6)$ $\dot{Q}_{SH,HP} = \dot{m}_{geo} \cdot c_{p,geo1} \cdot (T_{15} - T_{16})$ |
| Turbine | $\eta_T = \frac{h_5 - h_6}{h_5 - h_{6s}}$ $\dot{W}_T = \dot{m}_{wf} \cdot (h_5 - h_6) \cdot \eta_{m,T}$ | $\eta_{T,LP} = \frac{h_{11} - h_{12}}{h_{11} - h_{12s}}$ $\dot{W}_{T,LP} = \dot{m}_{wf} \cdot (h_{11} - h_{12}) \cdot \eta_{m,T}$ $\eta_{T,HP} = \frac{h_7 - h_8}{h_{17} - h_{8s}}$ $\dot{W}_{T,HP} = \dot{m}_{wf,HP} \cdot (h_7 - h_8) \cdot \eta_{m,T}$ |
| Desuperheater | $\dot{Q}_{DSH} = \dot{m}_{wf} \cdot (h_6 - h_7)$ $\dot{Q}_{DSH} = \dot{m}_{air} \cdot c_{p,air1} \cdot (T_{15} - T_{16})$ | $\dot{Q}_{DSH} = \dot{m}_{wf} \cdot (h_{12} - h_{13})$ $\dot{Q}_{DSH} = \dot{m}_{air} \cdot c_{p,air3} \cdot (T_{25} - T_{24})$ |
| Condenser | $\dot{Q}_{CON} = \dot{m}_{wf} \cdot (h_7 - h_8)$ $\dot{Q}_{CON} = \dot{m}_{air} \cdot c_{p,air2} \cdot (T_{14} - T_{15})$ | $\dot{Q}_{CON} = \dot{m}_{wf} \cdot (h_{13} - h_{14})$ $\dot{Q}_{CON} = \dot{m}_{air} \cdot c_{p,air2} \cdot (T_{24} - T_{23})$ |
| Subcooler | $\dot{Q}_{SC} = \dot{m}_{wf} \cdot (h_8 - h_1)$ $\dot{Q}_{SC} = \dot{m}_{air} \cdot c_{p,air3} \cdot (T_{14} - T_{13})$ | $\dot{Q}_{SC} = \dot{m}_{wf} \cdot (h_{14} - h_1)$ $\dot{Q}_{SC} = \dot{m}_{air} \cdot c_{p,air1} \cdot (T_{23} - T_{24})$ |
| Mixer/Splitter | | $\dot{m}_{wf,LP} \cdot h_{10} + \dot{m}_{wf,HP} \cdot h_{18} = \dot{m}_{wf} \cdot h_{11}$ $\dot{m}_{wf} = \dot{m}_{wf,LP} + \dot{m}_{wf,HP}$ |

Table A2. The relations for each component (first law analysis) for the DS parHTSLTPH ORC and DS HTSIHE ORC configurations.

| Configuration Component | DS parHTSLTPH ORC | DS HTSIHE ORC |
|-------------------------|---|---|
| Pump | $\eta_{p,LTS} = \frac{h_{22s} - h_{21}}{h_{22} - h_{21}}$ $\dot{W}_{p,LTS} = \frac{\dot{m}_{wf,LTS} \cdot (h_{22} - h_{21})}{\eta_{m,p}}$ $\eta_{p,HTS} = \frac{h_{23} - h_1}{h_2 - h_1}$ $\dot{W}_{p,HTS} = \frac{\dot{m}_{wf,HTS} \cdot (h_2 - h_1)}{\eta_{m,p}}$ | $\eta_{p,LTS} = \frac{h_{19s} - h_{18}}{h_{19} - h_{18}}$ $\dot{W}_{p,LTS} = \dot{m}_{wf,LTS} \cdot (h_{19} - h_{18})$ $\eta_{p,HTS} = \frac{h_{2s} - h_1}{h_2 - h_1}$ $\dot{W}_{p,HTS} = \frac{\dot{m}_{wf,HTS} \cdot (h_2 - h_1)}{\eta_{m,p}}$ |
| Preheater | $\dot{Q}_{PH,LTS} = \dot{m}_{wf,LTS} \cdot (h_{23} - h_{22})$ $\dot{Q}_{PH,LTS} = (1 - X_{HTS}) \cdot \dot{m}_{geo} \cdot c_{p,geo,PH,LTS} \cdot (T_{16} - T_{18})$ $\dot{Q}_{PH2,HTS} = \dot{m}_{wf,HTS} \cdot (h_4 - h_3)$ $\dot{Q}_{PH2,HTS} = \dot{m}_{geo} \cdot c_{p,geo,PH2,HTS} \cdot (T_{12} - T_{13})$ $\dot{Q}_{PH1,HTS} = \dot{m}_{wf,HTS} \cdot (h_2 - h_3)$ $\dot{Q}_{PH1,HTS} = \dot{m}_{geo} \cdot X_{HTS} \cdot c_{p,geo,PH1,HTS} \cdot (T_{17} - T_{19})$ | $\dot{Q}_{PH,LTS} = \dot{m}_{wf,LTS} \cdot (h_{20} - h_{15})$ $\dot{Q}_{PH,LTS} = \dot{m}_{geo} \cdot c_{p,geo,PH,LTS} \cdot (T_{16} - T_{17})$ $\dot{Q}_{PH,HTS} = \dot{m}_{wf,HTS} \cdot (h_4 - h_3)$ $\dot{Q}_{PH,HTS} = \dot{m}_{geo} \cdot c_{p,geo,PH,HTS} \cdot (T_{13} - T_{14})$ |
| Evaporator | $\dot{Q}_{EV,LTS} = \dot{m}_{wf,LTS} \cdot (h_{24} - h_{23})$ $\dot{Q}_{EV,LTS} = \dot{m}_{geo} \cdot c_{p,geo,EV,LTS} \cdot (T_{14} - T_{15})$ $\dot{Q}_{EV,HTS} = \dot{m}_{wf,HTS} \cdot (h_5 - h_4)$ $\dot{Q}_{EV,HTS} = \dot{m}_{geo} \cdot c_{p,geo,EV,HTS} \cdot (T_{11} - T_{12})$ | $\dot{Q}_{EV,LTS} = \dot{m}_{wf,LTS} \cdot (h_{21} - h_{20})$ $\dot{Q}_{EV,LTS} = \dot{m}_{geo} \cdot c_{p,geo,EV,LTS} \cdot (T_{15} - T_{16})$ $\dot{Q}_{EV,HTS} = \dot{m}_{wf,HTS} \cdot (h_5 - h_4)$ $\dot{Q}_{EV,HTS} = \dot{m}_{geo} \cdot c_{p,geo,EV,HTS} \cdot (T_{12} - T_{13})$ |
| Superheater | $\dot{Q}_{SH,LTS} = \dot{m}_{wf,LTS} \cdot (h_{25} - h_{24})$ $\dot{Q}_{SH,LTS} = \dot{m}_{geo} \cdot c_{p,geo,SH,LTS} \cdot (T_{13} - T_{14})$ $\dot{Q}_{SH,HTS} = \dot{m}_{wf,HTS} \cdot (h_6 - h_5)$ $\dot{Q}_{SH,HTS} = \dot{m}_{geo} \cdot c_{p,geo,SH,HTS} \cdot (T_{10} - T_{11})$ | $\dot{Q}_{SH,LTS} = \dot{m}_{wf,LTS} \cdot (h_{22} - h_{21})$ $\dot{Q}_{SH,LTS} = \dot{m}_{geo} \cdot c_{p,geo,SH,LTS} \cdot (T_{14} - T_{15})$ $\dot{Q}_{SH,HTS} = \dot{m}_{wf,HTS} \cdot (h_6 - h_5)$ $\dot{Q}_{SH,HTS} = \dot{m}_{geo} \cdot c_{p,geo,SH,HTS} \cdot (T_{11} - T_{12})$ |
| Turbine | $\eta_{T,LTS} = \frac{h_{25} - h_{26}}{h_{25} - h_{26s}}$ $\dot{W}_{T,LTS} = \dot{m}_{wf,LTS} \cdot (h_{25} - h_{26}) \cdot \eta_{m,T}$ $\eta_{T,HTS} = \frac{h_6 - h_7}{h_6 - h_{7s}}$ $\dot{W}_{T,HTS} = \dot{m}_{wf,HTS} \cdot (h_6 - h_7) \cdot \eta_{m,T}$ | $\eta_{T,LTS} = \frac{h_{22} - h_{23}}{h_{22} - h_{23s}}$ $\dot{W}_{T,LTS} = \dot{m}_{wf,LTS} \cdot (h_{22} - h_{23}) \cdot \eta_{m,T}$ $\eta_{T,HTS} = \frac{h_6 - h_7}{h_6 - h_{7s}}$ $\dot{W}_{T,HTS} = \dot{m}_{wf,HTS} \cdot (h_6 - h_7) \cdot \eta_{m,T}$ |
| Desuperheater | $\dot{Q}_{DSH,LTS} = \dot{m}_{wf,LTS} \cdot (h_{26} - h_{27})$ $\dot{Q}_{DSH,LTS} = \dot{m}_{air,LTS} \cdot c_{p,air,DSH,LTS} \cdot (T_{36} - T_{35})$ $\dot{Q}_{DSH,HTS} = \dot{m}_{wf,HTS} \cdot (h_7 - h_8)$ $\dot{Q}_{DSH,HTS} = \dot{m}_{air,HTS} \cdot c_{p,air,DSH,HTS} \cdot (T_{32} - T_{31})$ | $\dot{Q}_{DSH,LTS} = \dot{m}_{wf,LTS} \cdot (h_{23} - h_{24})$ $\dot{Q}_{DSH,LTS} = \dot{m}_{air,LTS} \cdot c_{p,air,DSH,LTS} \cdot (T_{33} - T_{32})$ $\dot{Q}_{DSH,HTS} = \dot{m}_{wf,HTS} \cdot (h_8 - h_9)$ $\dot{Q}_{DSH,HTS} = \dot{m}_{air,HTS} \cdot c_{p,air,DSH,HTS} \cdot (T_{29} - T_{28})$ |

Table A2. Cont.

| Configuration Component | DS parHTSLTPH ORC | DS HTSIHE ORC |
|-------------------------|--|---|
| Condenser | $\dot{Q}_{CON,LTS} = \dot{m}_{wf,LTS} \cdot (h_{27} - h_{28})$ | $\dot{Q}_{CON,LTS} = \dot{m}_{wf,LTS} \cdot (h_{24} - h_{25})$ |
| | $\dot{Q}_{CON,LTS} = \dot{m}_{air,LTS} \cdot c_{p,air,CON,LTS} \cdot (T_{35} - T_{34})$ | $\dot{Q}_{CON,LTS} = \dot{m}_{air,LTS} \cdot c_{p,air,CON,LTS} \cdot (T_{32} - T_{31})$ |
| | $\dot{Q}_{CON,HTS} = \dot{m}_{wf,HTS} \cdot (h_8 - h_9)$ | $\dot{Q}_{CON,HTS} = \dot{m}_{wf,HTS} \cdot (h_9 - h_{10})$ |
| | $\dot{Q}_{CON,HTS} = \dot{m}_{air,HTS} \cdot c_{p,air,CON,HTS} \cdot (T_{31} - T_{30})$ | $\dot{Q}_{CON,HTS} = \dot{m}_{air,HTS} \cdot c_{p,air,CON,HTS} \cdot (T_{28} - T_{27})$ |
| Subcooler | $\dot{Q}_{SC,LTS} = \dot{m}_{wf,LTS} \cdot (h_{28} - h_{21})$ | $\dot{Q}_{SC,LTS} = \dot{m}_{wf,LTS} \cdot (h_{25} - h_{18})$ |
| | $\dot{Q}_{SC,LTS} = \dot{m}_{air,LTS} \cdot c_{p,air,SC,LTS} \cdot (T_{34} - T_{33})$ | $\dot{Q}_{SC,LTS} = \dot{m}_{air,LTS} \cdot c_{p,air,SC,LTS} \cdot (T_{31} - T_{30})$ |
| | $\dot{Q}_{SC,HTS} = \dot{m}_{wf,HTS} \cdot (h_9 - h_1)$ | $\dot{Q}_{SC,HTS} = \dot{m}_{wf,HTS} \cdot (h_{10} - h_1)$ |
| | $\dot{Q}_{SC,HTS} = \dot{m}_{air,HTS} \cdot c_{p,air,SC,HTS} \cdot (T_{30} - T_{29})$ | $\dot{Q}_{SC,HTS} = \dot{m}_{air,HTS} \cdot c_{p,air,SC,HTS} \cdot (T_{27} - T_{26})$ |
| Mixer/Splitter | $X_{HTS} \cdot \dot{m}_{geo} \cdot h_{19} + (1 - X_{HTS}) \cdot \dot{m}_{geo} \cdot h_{18} = \dot{m}_{geo} \cdot h_{20}$ $\dot{m}_{geo} \cdot h_{15} = X_{HTS} \cdot \dot{m}_{geo} \cdot h_{17} + (1 - X_{HTS}) \cdot \dot{m}_{geo} \cdot h_{16}$ | |
| IHE | | $h_7 - h_8 = h_3 - h_2$ |

Table A3. The exergy relations used in the conventional exergy analysis for the SORC and DP ORC configurations.

| Configuration Component | SORC | | | DP ORC | | |
|-------------------------|-------------------------------|---------------------------------|-----------------|--|---|-----------------|
| | $\dot{E}_{F,k}$ | $\dot{E}_{P,k}$ | $\dot{E}_{L,k}$ | $\dot{E}_{F,k}$ | $\dot{E}_{P,k}$ | $\dot{E}_{L,k}$ |
| Pump | \dot{W}_P | $\dot{E}_2 - \dot{E}_1$ | | $\dot{W}_{P,LP}$ $\dot{W}_{P,HP}$ | $\dot{E}_2 - \dot{E}_1$ $\dot{E}_4 - \dot{E}_3$ | |
| Preheater | $\dot{E}_{11} - \dot{E}_{12}$ | $\dot{E}_3 - \dot{E}_2$ | \dot{E}_{12} | $\dot{E}_{20} - \dot{E}_{21}$ $\dot{E}_{17} - \dot{E}_{18}$ | $\dot{E}_3 - \dot{E}_4$ $\dot{E}_5 - \dot{E}_4$ | \dot{E}_{21} |
| Evaporator | $\dot{E}_{10} - \dot{E}_{11}$ | $\dot{E}_{X,4} - \dot{E}_{X,3}$ | | $\dot{E}_{19} - \dot{E}_{20}$ $\dot{E}_{16} - \dot{E}_{17}$ | $\dot{E}_5 - \dot{E}_3$ $\dot{E}_6 - \dot{E}_5$ | |
| Superheater | $\dot{E}_9 - \dot{E}_{10}$ | $\dot{E}_5 - \dot{E}_4$ | | $\dot{E}_{15} - \dot{E}_{16}$ | $\dot{E}_{10} - \dot{E}_9$ $\dot{E}_7 - \dot{E}_6$ | |
| Turbine | $\dot{E}_5 - \dot{E}_6$ | | | $\dot{E}_{11} - \dot{E}_{12}$ $\dot{E}_7 - \dot{E}_8$ | $\dot{W}_{T,LP}$ $\dot{W}_{T,HP}$ | |
| Condenser | $(\dot{E}_1 - \dot{E}_5)$ | $(\dot{E}_{15} - \dot{E}_{13})$ | \dot{E}_{16} | $(\dot{E}_{12} - \dot{E}_{11})$ | $(\dot{E}_{25} - \dot{E}_{22})$ | \dot{E}_{25} |
| Mixer/Splitter | | | | $\dot{E}_8 + \dot{E}_{10}$ | \dot{E}_{11} | |

Table A4. The exergy relations used in the conventional exergy analysis for the DS parHTSLTPH ORC and DS HTSIHE ORC configurations.

| Configuration Component | DS parHTSLTPH ORC | | | DS HTSIHE ORC | | |
|-------------------------|--|--|-----------------|--|--|-----------------|
| | $\dot{E}_{F,k}$ | $\dot{E}_{P,k}$ | $\dot{E}_{L,k}$ | $\dot{E}_{F,k}$ | $\dot{E}_{P,k}$ | $\dot{E}_{L,k}$ |
| Pump | $\dot{W}_{P,HTS}$ $\dot{W}_{P,LTS}$ | $\dot{E}_2 - \dot{E}_1$ $\dot{E}_{21} - \dot{E}_{22}$ | | $\dot{W}_{P,HTS}$ $\dot{W}_{P,LTS}$ | $\dot{E}_2 - \dot{E}_1$ $\dot{E}_{19} - \dot{E}_{18}$ | |

Table A4. Cont.

| Configuration Component | DS parHTSLTPH ORC | | | DS HTSIHE ORC | | |
|-------------------------|---------------------------------|---------------------------------|-----------------|-------------------------------|---------------------------------|-----------------|
| | $\dot{E}_{F,k}$ | $\dot{E}_{P,k}$ | $\dot{E}_{L,k}$ | $\dot{E}_{F,k}$ | $\dot{E}_{P,k}$ | $\dot{E}_{L,k}$ |
| Preheater | $\dot{E}_{12} - \dot{E}_{13}$ | $\dot{E}_4 - \dot{E}_3$ | | $\dot{E}_{13} - \dot{E}_{14}$ | $\dot{E}_2 - \dot{E}_3$ | |
| | $\dot{E}_{17} - \dot{E}_{19}$ | $\dot{E}_3 - \dot{E}_2$ | \dot{E}_{19} | | | |
| | $\dot{E}_{16} - \dot{E}_{18}$ | $\dot{E}_{23} - \dot{E}_{22}$ | \dot{E}_{18} | $\dot{E}_{16} - \dot{E}_{17}$ | $\dot{E}_{20} - \dot{E}_{19}$ | \dot{E}_{17} |
| Evaporator | $\dot{E}_{11} - \dot{E}_{12}$ | $\dot{E}_4 - \dot{E}_3$ | | $\dot{E}_{12} - \dot{E}_{13}$ | $\dot{E}_5 - \dot{E}_4$ | |
| | $\dot{E}_{13} - \dot{E}_{14}$ | $\dot{E}_{24} - \dot{E}_{23}$ | | $\dot{E}_{15} - \dot{E}_{16}$ | $\dot{E}_{21} - \dot{E}_{20}$ | |
| Superheater | $\dot{E}_{10} - \dot{E}_{11}$ | $\dot{E}_6 - \dot{E}_5$ | | $\dot{E}_{11} - \dot{E}_{12}$ | $\dot{E}_{X,6} - \dot{E}_{X,5}$ | |
| | $\dot{E}_{13} - \dot{E}_{14}$ | $\dot{E}_{25} - \dot{E}_{24}$ | | $\dot{E}_{14} - \dot{E}_{15}$ | $\dot{E}_{22} - \dot{E}_{21}$ | |
| Turbine | $\dot{E}_6 - \dot{E}_7$ | $\dot{W}_{T,HTS}$ | | $\dot{E}_6 - \dot{E}_7$ | $\dot{W}_{T,HTS}$ | |
| | $\dot{E}_{25} - \dot{E}_{26}$ | $\dot{W}_{T,LTS}$ | | $\dot{E}_{22} - \dot{E}_{23}$ | $\dot{W}_{T,LTS}$ | |
| Condenser | $(\dot{E}_{26} - \dot{E}_{21})$ | $(\dot{E}_{36} - \dot{E}_{33})$ | \dot{E}_{36} | $(\dot{E}_8 - \dot{E}_1)$ | $(\dot{E}_{29} - \dot{E}_{26})$ | \dot{E}_{29} |
| | $\dot{E}_7 - \dot{E}_1$ | $\dot{E}_{32} - \dot{E}_{26}$ | \dot{E}_{32} | $\dot{E}_{23} - \dot{E}_{12}$ | $\dot{E}_{33} - \dot{E}_{36}$ | \dot{E}_{33} |
| IHE | | | | $\dot{E}_7 + \dot{E}_8$ | $\dot{E}_3 - \dot{E}_2$ | |

Table A5. The obtained results of the net power optimization for the SORC configuration.

| SORC | | 120 °C | 140 °C | 160 °C | 180 °C |
|--------------|-----------|--------|--------|--------|--------|
| Cyclopentane | W_{net} | 13.52 | 22.33 | 33.54 | 47.36 |
| | P_{max} | 2.169 | 2.863 | 3.74 | 4.861 |
| n-Pentane | W_{net} | 13.61 | 22.71 | 34.49 | 49.37 |
| | P_{max} | 3.24 | 4.247 | 5.552 | 7.282 |
| Isopentane | W_{net} | 13.75 | 22.98 | 35 | 50.28 |
| | P_{max} | 4.059 | 5.28 | 6.857 | 8.969 |
| R1233zd(E) | W_{net} | 13.88 | 23.26 | 35.59 | 51.6 |
| | P_{max} | 5.858 | 7.669 | 10.09 | 13.59 |
| Neopentane | W_{net} | 13.95 | 23.52 | 32.29 | 53.34 |
| | P_{max} | 6.68 | 8.589 | 11.15 | 15.04 |
| R245fa | W_{net} | 14.09 | 23.78 | 36.75 | 54.25 |
| | P_{max} | 7.087 | 9.44 | 12.72 | 18.12 |
| n-butane | W_{net} | 13.9 | 23.44 | 36.24 | 53.77 |
| | P_{max} | 9.196 | 11.79 | 15.36 | 21.5 |
| R1234ze(Z) | W_{net} | 13.83 | 23.23 | 35.72 | 52.53 |
| | P_{max} | 7.678 | 10.04 | 13.35 | 19.03 |
| Isobutane | W_{net} | 14.08 | 24.06 | 38.24 | 67.23 |
| | P_{max} | 12.41 | 15.99 | 21.96 | 32.76 |
| R1234ze(E) | W_{net} | 14.63 | 27.36 | 48.58 | 59.89 |
| | P_{max} | 19.23 | 32.69 | 32.69 | 32.06 |
| R134a | W_{net} | 14.84 | 29.15 | 45.94 | 53.35 |
| | P_{max} | 25.84 | 36.53 | 36.53 | 33.01 |
| R1234yf | W_{net} | 15.74 | 31.03 | 41.81 | 34.69 |
| | P_{max} | 27.3 | 30.44 | 30.44 | 20.37 |

Table A6. The obtained results of the net power optimization for the DP ORC configuration.

| DP ORC | | 120 °C | 140 °C | 160 °C | 180 °C |
|--------------|----------------------|--------|--------|--------|--------|
| Cyclopentane | W_{net} | 17.38 | 28.24 | 41.75 | 57.96 |
| | $\Delta W_{netSORC}$ | 3.86 | 5.91 | 8.21 | 10.6 |
| | P_{HP} | 2.989 | 4.189 | 5.544 | 7.688 |
| | P_{LP} | 1.549 | 1.87 | 2.244 | 2.727 |
| | ΔT_{SHHP} | 5.287 | 5.468 | 5.001 | 5 |
| | ΔT_{SHLP} | 5.492 | 5.993 | 5.093 | 5.151 |
| n-Pentane | W_{net} | 17.15 | 28.04 | 41.64 | 58.1 |
| | $\Delta W_{netSORC}$ | 3.54 | 5.33 | 7.15 | 8.73 |
| | P_{HP} | 4.35 | 6.001 | 8.19 | 11 |
| | P_{LP} | 2.234 | 2.846 | 3.42 | 4.107 |
| | ΔT_{SHHP} | 5 | 5 | 5.17 | 5.017 |
| | ΔT_{SHLP} | 5.051 | 5.005 | 5.003 | 5.02 |
| Isopentane | W_{net} | 17.26 | 28.23 | 41.94 | 58.53 |
| | $\Delta W_{netSORC}$ | 3.51 | 5.25 | 6.94 | 8.25 |
| | P_{HP} | 5.38 | 7.329 | 9.941 | 13.25 |
| | P_{LP} | 2.954 | 3.569 | 4.297 | 5.136 |
| | ΔT_{SHHP} | 5.009 | 5.007 | 5.002 | 5.001 |
| | ΔT_{SHLP} | 5.003 | 5.001 | 5.004 | 5.067 |
| R1233zd(E) | W_{net} | 17.49 | 28.73 | 42.98 | 60.71 |
| | $\Delta W_{netSORC}$ | 3.61 | 5.47 | 7.39 | 9.11 |
| | P_{HP} | 7.786 | 10.73 | 14.56 | 20.81 |
| | P_{LP} | 4.267 | 5.18 | 6.275 | 7.89 |
| | ΔT_{SHHP} | 5.013 | 5.019 | 5.012 | 5.004 |
| | ΔT_{SHLP} | 5.056 | 5.044 | 5.111 | 5.021 |
| Neopentane | W_{net} | 17.3 | 28.38 | 42.39 | 59.82 |
| | $\Delta W_{netSORC}$ | 3.35 | 4.86 | 6.1 | 6.48 |
| | P_{HP} | 8.626 | 11.66 | 15.47 | 21.53 |
| | P_{LP} | 5.006 | 6.003 | 7.104 | 8.594 |
| | ΔT_{SHHP} | 5.001 | 5 | 5.001 | 5.002 |
| | ΔT_{SHLP} | 5.011 | 5.001 | 5.001 | 5.012 |
| R245fa | W_{net} | 17.63 | 29.05 | 43.63 | 68.79 |
| | $\Delta W_{netSORC}$ | 3.54 | 5.27 | 6.88 | 14.54 |
| | P_{HP} | 9.468 | 13.23 | 18.34 | 36.39 |
| | P_{LP} | 5.096 | 6.261 | 7.724 | 7.49 |
| | ΔT_{SHHP} | 5.004 | 5.002 | 5.008 | 5.021 |
| | ΔT_{SHLP} | 5.012 | 5 | 5.027 | 5.139 |
| DP ORC | | 120 °C | 140 °C | 160 °C | 180 °C |
| n-butane | W_{net} | 17.4 | 28.66 | 43.16 | 69.67 |
| | $\Delta W_{netSORC}$ | 3.5 | 5.22 | 6.92 | 15.9 |
| | P_{HP} | 11.83 | 15.76 | 22 | 37.96 |
| | P_{LP} | 6.923 | 8.221 | 10 | 10.2 |
| | ΔT_{SHHP} | 5 | 5.005 | 5 | 5.015 |
| | ΔT_{SHLP} | 5.001 | 5.001 | 5 | 5.014 |
| R1234ze(Z) | W_{net} | 17.5 | 28.82 | 43.31 | 62.67 |
| | $\Delta W_{netSORC}$ | 3.67 | 5.59 | 7.59 | 10.14 |
| | P_{HP} | 10.11 | 13.93 | 19.45 | 31.8 |
| | P_{LP} | 5.606 | 6.784 | 8.42 | 10.64 |
| | ΔT_{SHHP} | 5.058 | 5.075 | 5.01 | 5.004 |
| | ΔT_{SHLP} | 5.66 | 5.078 | 5.607 | 5.102 |
| Isobutane | W_{net} | 17.46 | 29 | 50 | 67.27 |
| | $\Delta W_{netSORC}$ | 3.38 | 4.94 | 11.84 | 0.04 |
| | P_{HP} | 15.7 | 21.13 | 36.4 | 32.76 |
| | P_{LP} | 9.454 | 11.31 | 11.21 | 6.904 |
| | ΔT_{SHHP} | 5 | 5.004 | 5.024 | 5.063 |
| | ΔT_{SHLP} | 5.014 | 5.006 | 6.02 | 9.138 |

Table A6. Cont.

| DP ORC | | 120 °C | 140 °C | 160 °C | 180 °C |
|------------|----------------------|--------|--------|--------|--------|
| R1234ze(E) | W_{net} | 17.87 | 31.07 | 47.6 | |
| | $\Delta W_{netSORC}$ | 3.24 | 3.71 | −0.98 | |
| | P_{HP} | 24.40 | 32.67 | 32.69 | |
| | P_{LP} | 14.22 | 15.49 | 9.021 | |
| | ΔT_{SHHP} | 5.035 | 5.005 | 5.828 | |
| | ΔT_{SHLP} | 5.003 | 5.229 | 5.927 | |
| R134a | W_{net} | 18.05 | 30.75 | | |
| | $\Delta W_{netSORC}$ | 3.21 | 1.6 | | |
| | P_{HP} | 32.98 | 36.52 | | |
| | P_{LP} | 18.9 | 16.51 | | |
| | ΔT_{SHHP} | 5.809 | 5.027 | | |
| | ΔT_{SHLP} | 6 | 7.257 | | |
| R1234yf | W_{net} | 18.58 | 30.97 | | |
| | $\Delta W_{netSORC}$ | 2.84 | −0.06 | | |
| | P_{HP} | 30.44 | 30.44 | | |
| | P_{LP} | 17 | 9.079 | | |
| | ΔT_{SHHP} | 5 | 5.019 | | |
| | ΔT_{SHLP} | 5 | 6.588 | | |

Table A7. Thermodynamic states of the working fluids, geothermal fluid (water), and cooling fluid (air) in characteristic points of the DS parHTSLTPH ORC configuration with R1234yf in HTS and LTS stages for a geothermal fluid temperature of 120 °C.

| State | Fluid | T (°C) | P (bar) | H (kJ/kg) | S (kJ/kgK) | M (kg/s) |
|-------|----------|--------|---------|-----------|------------|----------|
| 1 | wf HTS | 33 | 8.952 | 244.8 | 1.153 | 1.273 |
| 2 | | 35.2 | 30.44 | 247.6 | 1.156 | |
| 3 | | 62.07 | 30.44 | 287.4 | 1.279 | |
| 4 | | 89.41 | 30.44 | 341.1 | 1.433 | |
| 5 | | 89.41 | 30.44 | 394.3 | 1.579 | |
| 6 | | 94.41 | 30.44 | 409.5 | 1.621 | |
| 7 | | 41.81 | 8.952 | 392.1 | 1.631 | |
| 8 | | 35 | 8.952 | 384.6 | 1.606 | |
| 9 | | 35 | 8.952 | 247.6 | 1.162 | |
| 10 | geofluid | 120 | 10 | 504.4 | 1.527 | 1 |
| 11 | | 115.4 | 10 | 485 | 1.478 | |
| 12 | | 99.41 | 10 | 417.3 | 1.3 | |
| 13 | | 83.15 | 10 | 349 | 1.112 | |
| 14 | | 82.46 | 10 | 346.1 | 1.104 | |
| 15 | | 72.07 | 10 | 302.5 | 0.9789 | |
| 16 | | 72.07 | 10 | 302.5 | 0.9789 | |
| 17 | | 72.07 | 10 | 302.5 | 0.9789 | |
| 18 | | 42.86 | 10 | 180.4 | 0.61 | |
| 19 | | 57.95 | 10 | 243.4 | 0.805 | |
| 20 | | 55.8 | 10 | 234.4 | 0.777 | |

Table A7. *Cont.*

| State | Fluid | T (°C) | P (bar) | H (kJ/kg) | S (kJ/kgK) | M (kg/s) |
|-------|--------|--------|---------|-----------|------------|----------|
| 21 | wf LTS | 33 | 8.952 | 244.8 | 1.153 | 0.4046 |
| 22 | | 33.86 | 17.2 | 245.9 | 1.154 | |
| 23 | | 62.07 | 17.2 | 289 | 1.288 | |
| 24 | | 62.07 | 17.2 | 396.6 | 1.609 | |
| 25 | | 67.07 | 17.2 | 403.7 | 1.63 | |
| 26 | | 43.29 | 8.952 | 393.7 | 1.636 | |
| 27 | | 35 | 8.952 | 384.6 | 1.606 | |
| 28 | | 35 | 8.952 | 247.6 | 1.162 | |
| 29 | | 20 | 1 | 293.3 | 6.845 | |
| 30 | 20.19 | 1 | 293.5 | 6.846 | | |
| 31 | 29.49 | 1 | 302.9 | 6.878 | | |
| 32 | 30 | 1 | 303.4 | 6.879 | | |
| 33 | air | 20 | 1 | 293.3 | 6.845 | 5.989 |
| 34 | | 20.19 | 1 | 293.5 | 6.846 | |
| 35 | | 29.39 | 1 | 302.8 | 6.877 | |
| 36 | | 30 | 1 | 303.4 | 6.879 | |

Table A8. Thermodynamic states of the working fluids, geothermal fluid (water), and cooling fluid (air) in characteristic points of the DS HTSIHE ORC configuration with R1234yf in HTS and LTS stages for a geothermal fluid temperature of 120 °C.

| State | Fluid | T (°C) | P (bar) | h (kJ/kg) | s (kJ/kgK) | m (kg/s) |
|-------|----------|--------|---------|-----------|------------|----------|
| 1 | wf HTS | 33 | 8.952 | 244.8 | 1.153 | 0.928 |
| 2 | | 35.06 | 29.02 | 247.5 | 1.155 | |
| 3 | | 53.03 | 29.02 | 273.6 | 1.238 | |
| 4 | | 87.01 | 29.02 | 335.2 | 1.417 | |
| 5 | | 87.01 | 29.02 | 396.3 | 1.586 | |
| 6 | | 110 | 29.02 | 439.9 | 1.704 | |
| 7 | | 67.16 | 8.952 | 419.6 | 1.715 | |
| 8 | | 43.06 | 8.952 | 393.5 | 1.635 | |
| 9 | | 35 | 8.952 | 384.6 | 1.606 | |
| 10 | | 35 | 8.952 | 247.6 | 1.162 | |
| 11 | geofluid | 120 | 10 | 504.4 | 1.527 | 1 |
| 12 | | 110.5 | 10 | 464 | 1.423 | |
| 13 | | 97.01 | 10 | 407.3 | 1.273 | |
| 14 | | 83.4 | 10 | 350 | 1.115 | |
| 15 | | 82.49 | 10 | 346.2 | 1.104 | |
| 16 | | 66.81 | 10 | 280.5 | 0.9155 | |
| 17 | | 62.03 | 10 | 260.5 | 0.8562 | |

Table A8. Cont.

| State | Fluid | T (°C) | P (bar) | h (kJ/kg) | s (kJ/kgK) | m (kg/s) |
|-------|--------|--------|---------|-----------|------------|----------|
| 18 | wf LTS | 33 | 8.952 | 244.8 | 1.153 | 0.5746 |
| 19 | | 33.66 | 15.27 | 245.6 | 1.154 | |
| 20 | | 56.81 | 15.27 | 280.5 | 1.263 | |
| 21 | | 56.81 | 15.27 | 394.8 | 1.61 | |
| 22 | | 61.81 | 15.27 | 401.5 | 1.63 | |
| 23 | | 42.85 | 8.952 | 393.2 | 1.634 | |
| 24 | | 35 | 8.952 | 384.6 | 1.606 | |
| 25 | | 35 | 8.952 | 247.6 | 1.162 | |
| 26 | | 20 | 1 | 293.3 | 6.845 | |
| 27 | | 20.19 | 1 | 293.5 | 6.846 | |
| 28 | 29.4 | 1 | 302.8 | 6.877 | | |
| 29 | 30 | 1 | 303.4 | 6.879 | | |
| 30 | air | 20 | 1 | 293.3 | 6.845 | 8.478 |
| 31 | | 20.2 | 1 | 293.5 | 6.846 | |
| 32 | | 29.42 | 1 | 302.8 | 6.877 | |
| 33 | | 30 | 1 | 303.4 | 6.879 | |

References

- Loni, R.; Mahian, O.; Najafi, G.; Sahin, A.Z.; Rajaei, F.; Kasaeian, A.; Mehrpooya, M.; Bellos, E.; le Roux, W.G. A critical review of power generation using geothermal-driven organic Rankine cycle. *Therm. Sci. Eng. Prog.* **2021**, *25*, 101028. [\[CrossRef\]](#)
- Astolfi, M.; Romano, M.C.; Bombarda, P.; Macchi, E. Binary ORC (Organic Rankine Cycles) power plants for the exploitation of medium-low temperature geothermal sources—Part A: Thermodynamic optimization. *Energy* **2014**, *66*, 423–434. [\[CrossRef\]](#)
- Liu, Q.; Duan, Y.; Yang, Z. Performance analyses of geothermal organic Rankine cycles with selected hydrocarbon working fluids. *Energy* **2013**, *63*, 123–132. [\[CrossRef\]](#)
- Jouhara, H.; Khordehghah, N.; Almahmoud, S.; Delpech, B.; Chauhan, A.; Tassou, S.A. Waste heat recovery technologies and applications *Therm. Sci. Eng. Prog.* **2018**, *6*, 268–289.
- Moya, D.; Aldás, C.; Kaparaju, P. Geothermal energy: Power plant technology and direct heat applications *Renew. Sustain. Energy Rev.* **2018**, *94*, 889–901. [\[CrossRef\]](#)
- DiPippo, R. Chapter 8. Binary Cycle Power Plant. In *Geothermal Power Plant Principles, Applications, Case Studies and Environmental Impact*; Elsevier Ltd.: Amsterdam, The Netherlands, 2015; pp. 193–239.
- Nemati, A.; Nami, H.; Ranjbar, F.; Yari, M. Case Studies in Thermal Engineering A comparative thermodynamic analysis of ORC and Kalina cycles for waste heat recovery: A case study for CGAM cogeneration system. *Case Stud. Therm. Eng.* **2017**, *9*, 1–13. [\[CrossRef\]](#)
- Lecompte, S.; Huisseune, H.; van den Broek, M.; Vanslambrouck, B.; De Paepe, M. Review of organic Rankine cycle (ORC) architectures for waste heat recovery. *Renew. Sustain. Energy Rev.* **2015**, *47*, 448–461. [\[CrossRef\]](#)
- Stijepovic, M.Z.; Papadopoulos, A.I.; Linke, P.; Grujic, A.S.; Seferlis, P. An exergy composite curves approach for the design of optimum multi-pressure organic Rankine cycle processes. *Energy* **2014**, *69*, 285–298. [\[CrossRef\]](#)
- Li, T.; Zhang, Z.; Lu, J.; Yang, J.; Hu, Y. Two-Stage Evaporation Strategy to Improve System Performance for Organic Rankine Cycle. *Appl. Energy* **2015**, *150*, 323–334. [\[CrossRef\]](#)
- Li, J.; Ge, Z.; Liu, Q.; Duan, Y.Y.; Yang, Z. Thermo-economic performance analyses and comparison of two turbine layouts for organic Rankine cycles with dual-pressure evaporation. *Energy Convers. Manag.* **2018**, *164*, 603–614. [\[CrossRef\]](#)
- Guzovic, Z.; Raskovic, P.; Blataric, Z. The comparison of a basic and a dual-pressure ORC (Organic Rankine Cycle): Geothermal Power Plant Velika Ciglena case study. *Energy* **2014**, *76*, 175–186. [\[CrossRef\]](#)
- Manante, G.; Lazzaretto, A.; Bonamico, E. Design guidelines for the choice between single and dual pressure layouts in organic Rankine cycle (ORC) systems. *Energy* **2017**, *123*, 413–431. [\[CrossRef\]](#)
- Li, X.; Liu, T.; Chen, L. Thermodynamic Performance Analysis of an Improved Two-Stage Organic Rankine Cycle. *Energies* **2018**, *11*, 2864. [\[CrossRef\]](#)
- Ayachi, F.; Ksayer, E.B.; Zoughaib, A.; Neveu, P. ORC optimization for medium grade heat recovery. *Energy* **2014**, *68*, 47–56. [\[CrossRef\]](#)
- Braimakis, K.; Karellas, S. Exergetic optimization of double stage Organic Rankine Cycle. *Energy* **2018**, *149*, 296–313. [\[CrossRef\]](#)

17. Kanoglu, M. Exergy analysis of a dual-level binary geothermal power plant. *Geothermics* **2002**, *31*, 709–724. [[CrossRef](#)]
18. Heberle, F.; Jahrfeld, T.; Brüggemann, D. Thermodynamic Analysis of Double-Stage Organic Rankine Cycles for Low-Enthalpy Sources Based on a Case Study for 5.5 MWe Power Plant Kirchstockach (Germany). In Proceedings of the World Geothermal Congress 2015, Melbourne, Australia, 19–25 April 2015.
19. Liu, G.; Wang, Q.; Xu, J.; Miao, Z. Exergy Analysis of Two-Stage Organic Rankine Cycle Power Generation System. *Entropy* **2021**, *23*, 43. [[CrossRef](#)]
20. Ge, Z.; Li, J.; Duan, Y.; Yang, Z.; Xie, Z. Thermodynamic Performance Analyses and Optimization of Dual-Loop Organic Rankine Cycles for Internal Combustion Engine Waste Heat Recovery. *Appl. Sci.* **2019**, *9*, 680. [[CrossRef](#)]
21. Song, J.; Gu, C. Parametric analysis of a dual loop Organic Rankine Cycle (ORC) system for engine waste heat recovery. *Energy Convers. Manag.* **2015**, *105*, 995–1005. [[CrossRef](#)]
22. Nami, H.; Nemati, A.; Fard, F.J. Conventional and advanced exergy analyses of a geothermal driven dual fluid organic Rankine cycle (ORC). *Appl. Therm. Eng.* **2017**, *122*, 59–70. [[CrossRef](#)]
23. Klein, S.A. *EES, Engineering Equation Solver*; Versio: Madison, WI, USA, 2004.
24. Chen, H.; Goswami, D.Y.; Stefanakos, E.K. A review of thermodynamic cycles and working fluids for the conversion of low-grade heat. *Renew. Sustain. Energy Rev.* **2010**, *14*, 3059–3067. [[CrossRef](#)]
25. Hu, K.; Zhu, J.; Zhang, W.; Liu, K.; Lu, X. Effects of evaporator superheat on system operation stability of an organic Rankine cycle. *Appl. Therm. Eng.* **2017**, *111*, 793–801. [[CrossRef](#)]
26. Seider, W.D.; Seader, J.D.; Lewin, D.R. *Product & Process Design Principles: Synthesis, Analysis and Evaluation*; John Wiley & Sons: Hoboken, NJ, USA, 2009.
27. Groniewsky, A.; Györke, G.; Imre, A.R. Description of wet-to-dry transition in model ORC working fluids. *Appl. Therm. Eng.* **2017**, *125*, 963–971. [[CrossRef](#)]
28. *Montreal Protocol on Substances that Deplete the Ozone Layer*; US Government Printing Office: Washington, DC, USA, 1987; pp. 128–136.
29. Yang, J.; Gao, L.; Ye, Z.; Hwang, Y.; Chen, J. Binary-objective optimization of latest low-GWP alternatives to R245fa for organic Rankine cycle application. *Energy* **2021**, *217*, 119336. [[CrossRef](#)]
30. Liu, W.; Meinel, D.; Wieland, C.; Spliethoff, H. Investigation of hydro fluoroolefins as potential working fluids in organic Rankine cycle for geothermal power generation. *Energy* **2014**, *67*, 106–116. [[CrossRef](#)]
31. Eyerer, S.; Dawo, F.; Kaind, J.; Wieland, C.; Spliethoff, H. Experimental investigation of modern ORC working fluids R1224yd(Z) and R1233zd(E) as replacements for R245fa. *Appl. Energy* **2019**, *240*, 946–963. [[CrossRef](#)]
32. Bahrami, M.; Pourfayaz, F.; Kasaeian, A. Low global warming potential (GWP) working fluids (WFs) for Organic Rankine Cycle (ORC) applications. *Energy Rep.* **2022**, *8*, 2976–2988. [[CrossRef](#)]
33. Noriega Sanchez, C.J.; Gosselin, L.; da Silva, A.K. Designed binary mixtures for subcritical organic Rankine cycles based on multiobjective optimization. *Energy Convers. Manag.* **2018**, *156*, 585–596. [[CrossRef](#)]